A Comparison of Numerical Solutions for Advection-Diffusion-Reaction Equations between Finite Volume and Finite Difference Methods

Kanokwarun Para, Surattana Sungnul, Sekson Sirisubtawee and Sutthisak Phongthanapanich

***Abstract*—In this article, an explicit characteristic-based finite volume method (FVM) is presented for the numerical solution of advection-diffusion-reaction equations (ADRE). The method was applied to solve 1-D and 2-D water pollution problems which can be modeled in terms of ADREs. The FVM results were compared with numerical results obtained using a finite difference method (FDM) with implicit forward time central space (FTCS) scheme. For the 1-D ADRE, numerical solutions from the two methods were also compared with the exact solution. Good agreement was found between the FVM, FDM and exact results for the 1-D ADRE. The FVM and FDM methods were also used to obtain numerical solutions for 2-D ADRE models for water pollution in reservoirs with one or two entrance gates and one exit gate for low and high rates of diffusion for three representative source terms. In general, it was found that the FVM and FDM results were in good agreement except for regions near the entrance and exit gates.**

***Index Terms*—Water pollutant concentration, Finite volume method, Finite difference method, Advection-diffusion-reaction equation**

I. Introduction

ACCURATE numerical solutions of advection-diffusion-reaction equations (ADRE) play a vital role in the modeling of physical processes as the equations are used as models for many problems arising in applied mathematics, science and engineering, for example, heat transfer, water pollutant concentration, air pollutant concentration, etc. Two important numerical methods that have been developed to solve ADREs are finite difference methods (FDM) (see, e.g., [1]–[7]) and finite volume methods (FVM) (see, e.g., [8]–[21]).

Many researchers have used finite difference methods to numerically solve partial differential equations related to ADREs. Some examples include the following. In 2013, Gurarslan et al. [2] published numerical solutions of contaminant transport problems written in terms of a 1-D advection-diffusion equation by using a sixth-order compact finite difference scheme in space and a fourth-order Runge-Kutta scheme in time. This combined method was shown to give very reliable and accurate solutions to these problems. In 2014, Qin et al. [3] proposed a non-standard finite difference (NSFD) scheme to solve an advection-reaction equation with a nonlinear reaction term. Qin et al. also used the new scheme to construct numerical solutions of the advection-reaction equations both with and without a diffusion term. They showed that the NSFD scheme could preserve the fixed points, the positivity, and the boundedness of the solutions of the original equations. In 2017, Sanjaya and Mungkasi [4] developed an explicit finite difference method to obtain numerical solutions of a 1-D advection-diffusion equation. In 2018, Putri et al. [5] used numerical simulations to study an advection-diffusion equation for the Biochemical Oxygen Demand (BOD) concentration in one flow direction in waste stabilization ponds. The numerical simulations were carried out using a finite difference method with a forward time central space (FTCS) scheme. In 2020, Pananu et al. [1] analyzed the convergence of a finite difference method with an implicit forward time central space (FTCS) scheme for numerical solution of a 2-D advection-diffusion-reaction equation. Pananu et al. also applied the scheme to a water pollutant dispersion problem with non-removal and removal mechanisms in reservoirs with one and two entrance gates. In 2020, Xu et al. [6] used a reduced sixth-order compact finite difference scheme (R-CFDS6) to solve the 2-D Fisher-Kolmogorov equation and an extended Fisher-Kolmogorov equation. Their scheme was based on proper orthogonal decomposition (POD) and operator splitting (R-CFDS6-OSM). In 2020, Timpitak and Pochai [7] published numerical results which they obtained using forward time central space and Saulyev finite difference techniques to solve a 1-D model of groundwater pollution measurements around heterogeneous soil landfills.

In recent years, many researchers have made detailed studies of the finite volume method. Some examples include the following. In 2014, Arachchige and Pettet [15] proposed a new linearization technique, which they called the finite volume method with linearization (FVML), for temporal integration of nonlinear source terms in an ADRE . They also applied the FVML to obtain numerical simulations of a variety of 1-D ADREs. In 2015, Liu et al. [16] developed a modified upwind finite volume element method to decompose a nonlinear system into a smaller nonlinear system on a coarse grid and a linear system on a fine grid. Liu et al. then

Manuscript received July 30, 2021; revised Feb 1, 2022. This research was funded by the Science Achievement Scholarship of Thailand (SAST).

Kanokwarun Para is a Ph.D student in Applied Mathematics, King Mongkut's University of Technology North Bangkok, 10800 THAILAND (e-mail: kanokwan.kanok@gmail.com).

Surattana Sungnul is Associate Professor in the Department of Mathematics, King Mongkut's University of Technology North Bangkok, 10800 THAILAND and researcher in the Center of Excellence in Mathematics, 10400 THAILAND (corresponding author, e-mail: surattana.s@sci.kmutnb.ac.th).

Sekson Sirisubtawee is Associate Professor in the Department of Mathematics, King Mongkut's University of Technology North Bangkok, 10800 THAILAND and researcher in the Center of Excellence in Mathematics, 10400 THAILAND (e-mail: sekson.s@sci.kmutnb.ac.th).

Sutthisak Phongthanapanich is Professor in the Department of Mechanical Engineering Technology, College of Industrial Technology, King Mongkut's University of Technology North Bangkok 10800 THAILAND (e-mail: sutthisak.p@cit.kmutnb.ac.th).

applied their method to solve a system of coupled advection-dominated diffusion reaction equations for the prevention of groundwater contamination. In 2017, Yang and Tine [17] proposed a hybrid finite volume scheme based on a flux convex combination between the Anti-Dissipative Method (ADM) [22] and the WENO5 method [23]. Yang and Tine used their scheme to construct accurate numerical solutions of transport type equations for discontinuous initial data. This hybrid scheme was shown to be very suitable for deriving long term asymptotic behavior of solutions of population dynamic models. In 2018, Xu [18] proposed a modified finite volume method (MFVM) in which the weights of the upstream and downstream grid points were adjusted to minimize the truncation errors. Xu showed that the MFVM was much more accurate and stable than the conventional FVM for convection/reaction-dominated problems and provided almost the same accuracy as the exact solution. In addition, they showed that the MVFM did not induce any unphysical oscillations for the 1-D case. In 2019, Lan et al. [19] introduced a new finite volume scheme for 2-D convection-diffusion equations on deformed meshes in which the convective flux was approximated using the available information on the diffusive flux. The scheme was shown to be appropriate for cases in which the diffusion coefficients were discontinuous and anisotropic. In addition, it was shown that the scheme preserved the positivity of solutions, had second-order accuracy, and did not require special slope-limiting techniques. Hafsi and Taallah [20] used a finite volume method to obtain approximate solutions of the Signorini problem for a deformed elastic solid in unilateral contact with a rigid body. More recently, Hussain et al. [21] developed a numerical scheme based on the upwind approach in the finite volume method. They proposed new expressions for interface flux approximations and showed that their proposed scheme was unconditionally stable with second-order accuracy in both space and time. Also, they obtained highly accurate solutions for the convection-diffusion problem with a range of values of convective velocity and diffusion coefficient.

In this article, advection-diffusion-reaction equations of the following form are studied:

$$\frac{\partial \phi}{\partial t} + \nabla \cdot (\mathbf{v}\phi - \varepsilon \nabla \phi) + \kappa \phi = q, \tag{1}$$

where ϕ is a scalar quantity such as water pollutant concentration or air pollutant concentration, the symbol ∇ represents the gradient operator, $\varepsilon \geq 0$ is a diffusion coefficient, $\mathbf{v} = \mathbf{v(x)}$ is a given advection velocity vector, κ is a reaction coefficient, $q = q(\mathbf{x}, t)$ is a prescribed source term, $\mathbf{x} = (x_1, x_2, ..., x_k)^T$ is a position vector of k components and time $t \in [0, T]$, where $T > 0$.

The purpose of the current work is to develop an explicit characteristic-based finite volume scheme [8]–[14] to obtain numerical solutions of Eq. (1) for a model of water pollution problems in a reservoir. The numerical simulations obtained by the proposed finite volume method are compared with the solutions reported in [1] that were obtained by a finite difference method with an implicit forward time central space (FTCS) scheme. The accuracy of the two numerical methods will first be tested by applying them to a simple one-dimensional water pollution problem for which an exact solution is known. The two methods will then be used to solve a two-dimensional water pollution problem for which an exact solution is not known.

The present paper is organized as follows. In section II, a summary is given of the finite difference method with implicit FTCS scheme discussed in [1]. The explicit characteristic-based finite volume method is then described and its application to the solution of pure advection and advection-dominated diffusion problems is summarized [8], [9], [12], [13]. In section III, numerical solutions for the 1-D ADREs for the water pollution problems are obtained using the two methods and compared with the exact solution. Then, numerical solutions for the 2-D ADREs are obtained using the two methods and extensive graphs are presented to illustrate the numerical results. Finally, conclusions are given in section IV.

II. Numerical Methods

In this section, the main properties of the finite difference method with implicit FTCS scheme and the explicit characteristic-based finite volume method are summarized.

A. Finite difference method with implicit FTCS scheme

The finite difference method with the implicit FTCS scheme for the 2-D version of the advection-diffusion-reaction equation (1) is as follows [1]:

$$\begin{aligned} L_h\phi^h(\mathbf{x},t) \equiv & \frac{\phi_{i,j}^{n+1} - \phi_{i,j}^{n}}{\Delta t} + \bar{u}\frac{\phi_{i+1,j}^{n+1} - \phi_{i-1,j}^{n+1}}{2\Delta x} + \bar{v}\frac{\phi_{i,j+1}^{n+1} - \phi_{i,j-1}^{n+1}}{2\Delta y} \\ & -\varepsilon\left[\frac{\phi_{i+1,j}^{n+1} - 2\phi_{i,j}^{n+1} + \phi_{i-1,j}^{n+1}}{(\Delta x)^2} + \frac{\phi_{i,j+1}^{n+1} - 2\phi_{i,j}^{n+1} + \phi_{i,j-1}^{n+1}}{(\Delta y)^2}\right] \\ & + \kappa\phi_{i,j}^{n+1} = q_{i,j}^{n}, \end{aligned} \tag{2}$$

where $L_h : \Omega_h \to H_h$ is a difference operator acting from the discrete function space Ω_h to the discrete function space H_h. The discretized function $\phi^h \in \Omega_h$ is written in terms of the solution ϕ, where $\phi^h(\mathbf{x}, t) = \phi_{i,j}^n = \phi(x_i, y_j, t^n)$ and $(i, j) \in J = \{(i, j) \mid i = 0, 1, 2, ..., N_1,\ j = 0, 1, 2, ..., N_2\}$ are the space points and $n \in K = \{0, 1, 2, ..., N\}$ are the time points. The positive integers N_1 and N_2 are computed via $N_1 = \frac{L_1}{\Delta x}$, $N_2 = \frac{L_2}{\Delta y}$, where L_1, Δx and L_2, Δy are the side length of the considered region and the spatial step sizes in x- and y-directions, respectively. The interval of time $[0, T]$ is discretized as $[0, T]_K$, where t_n, $n \in K = \{0, 1, 2, ..., N\}$ are the temporal grid points with step size $\Delta t = T/N$ for some positive integer N. The symbols $\bar{u}$ and $\bar{v}$ are the average advection velocities in x- and y-directions, respectively.

Pananu et al. [1] established that the scheme (2) is convergent, i.e., consistent and stable, by Lax's equivalence theorem [24]. In particular, the magnitude of the eigenvalue (λ) of the discretized solution $\phi_{i,j}^n$ for the homogeneous scheme of (2) was shown to be given by [1]

$$\begin{aligned} |\lambda| = & \frac{1}{\sqrt{\left[1+\gamma\left(\sin^2\frac{\alpha}{2} + \sin^2\frac{\beta}{2}\right)+\kappa\tau\right]^2 + \left[\eta\left(\bar{u}\sin\alpha + \bar{v}\sin\beta\right)\right]^2}}, \\ \leq & \ 1, \end{aligned} \tag{3}$$

where $\gamma = \frac{4\varepsilon\tau}{h^2}$, $\eta = \frac{\tau}{h}$ and $\tau = \Delta t$, $h = \Delta x = \Delta y$. The unconditional Von Neumann stability for the homogeneous scheme can then be directly proved using the inequality (3).

In addition, it can easily be shown that the 1-D homogeneous scheme of (2), i.e., without $\bar{v}$ and κ, is unconditionally stable. For the nonhomogeneous case, the scheme (2) is stable if the following hypothesis holds [1]:

$$(\mathbf{H1})\begin{cases} \bar{u}\left[\phi^{n+1}_{i^*-1,j^*} - \phi^{n+1}_{i^*+1,j^*}\right] \leq 0, \\ \bar{v}\left[\phi^{n+1}_{i^*,j^*-1} - \phi^{n+1}_{i^*,j^*+1}\right] \leq 0, \end{cases} \tag{4}$$

where (i^*, j^*) are the smallest non-negative integers in J.

B. Explicit characteristic-based finite volume method

The idea of the method is to first derive a discrete convection-diffusion-reaction equation along a characteristic path and then to use the weighted residuals finite element method to approximate the gradients on the cell faces [8], [12], [13].

The derivation of the method for solving equation (1) can be summarized as follows. Consider the initial-boundary value problem for the ADRE consisting of the governing equation (1), the initial condition

$$\phi(\mathbf{x}, 0) = \phi_0(\mathbf{x}), \quad \mathbf{x} \in \Omega, \quad \Omega \subset \mathbb{R}^2, \tag{5}$$

and the Dirichlet and Neumann boundary conditions

$$\begin{aligned} \phi(\mathbf{x}, t) &= g_D \quad \text{on} \quad \partial\Omega_D, \\ \varepsilon\frac{\partial\phi}{\partial\mathbf{n}} &= g_N \quad \text{on} \quad \partial\Omega_N, \end{aligned} \tag{6}$$

where Ω is a bounded polygonal spatial domain with the Lipschitz boundary, i.e., $\partial\Omega = \partial\Omega_D \cup \partial\Omega_N$ and $\partial\Omega_D \cap \partial\Omega_N = \emptyset$, where $\partial\Omega_D$ and $\partial\Omega_N$ are the Dirichlet and Neumann boundaries, respectively. In addition, g_D and g_N are specified function spaces on Ω_D and Ω_N, respectively and $\mathbf{n}$ is the unit outward normal vector.

If a moving coordinate $\mathbf{x}'$ with a speed of $\mathbf{v}$ is assumed along the path of the characteristic wave, then the change of variable $\mathbf{x}$ to $\mathbf{x}'$ is expressed by $\mathbf{x}' = \mathbf{x} - \mathbf{v}t$. Then, if $\phi = \phi(\mathbf{x}', t)$, the relation between the derivatives is as follows:

$$\left.\frac{\partial\phi}{\partial t}\right|_{\mathbf{x}=\text{constant}} = -\mathbf{v}\cdot\nabla'\phi + \left.\frac{\partial\phi}{\partial t}\right|_{\mathbf{x}'=\text{constant}}, \tag{7}$$

$$\nabla\phi = \nabla'\phi, \tag{8}$$

$$\nabla\cdot(\varepsilon\nabla\phi) = \nabla'\cdot(\varepsilon\nabla'\phi). \tag{9}$$

After substituting (7)-(9) into (1) and using the divergence free assumption that $\nabla\cdot\mathbf{v} = 0$, the advection term in Eq. (1) disappears and Eq. (1) then becomes

$$\frac{\partial\phi}{\partial t} - \nabla'\cdot(\varepsilon\nabla'\phi) + \kappa\phi = q, \tag{10}$$

where all terms are evaluated at $\mathbf{x}'=\mathbf{x}'(t)$.

The next step is to discretize the computational domain in time and space. The time interval $[0, T]$ is discretized with a time step Δt and then the time steps are $t^n = n\Delta t,\ n = 0, 1, 2, \ldots, N$. Then, by carrying out a Taylor-series expansion to second order in time, the advection term reappears in the equation along with an additional second-order term. This second-order term acts as a smoothing operator that reduces the oscillations arising from the spatial discretization of the advection term. For convenience, ∇ will be used instead of ∇' for the remaining steps. Then, the full explicit characteristic advection-diffusion-reaction equation is given by

$$\begin{aligned} \phi^{n+1} - \phi^n &= -\Delta t\left[(\mathbf{v}\cdot\nabla\phi^n) - \varepsilon\nabla\cdot\nabla\phi^n + \kappa\phi - q\right] \\ &\quad + \frac{(\Delta t)^2}{2}\mathbf{v}\cdot\nabla\left(\mathbf{v}\cdot\nabla\phi^n + \kappa\phi - q\right). \end{aligned} \tag{11}$$

Finally, using the divergence free assumption, Eq. (11) can be written in the conservation form:

$$\begin{aligned} \phi^{n+1} - \phi^n &= -\Delta t\left[\nabla\cdot(\mathbf{v}\phi^n - \varepsilon\nabla\phi^n) + \kappa\phi - q\right] \\ &\quad + \frac{(\Delta t)^2}{2}\nabla\cdot\left[\mathbf{v}\left(\mathbf{v}\cdot\nabla\phi^n + \kappa\phi - q\right)\right]. \end{aligned} \tag{12}$$

The computational domain for space is discretized into a collection of non-overlapping control volumes $\Omega_i \subset \Omega,\ i = 1, ..., N$, that completely cover the domain Ω such that $\Omega = \cup_{i=1}^{N}\Omega_i,\ \Omega_i \neq \emptyset$ and $\Omega_i \cap \Omega_j = \emptyset$ if $i \neq j$. Then, to obtain the finite volume equation, Eq. (12) is integrated over each control volume Ω_i to yield

$$\begin{aligned} \int_{\Omega_i}\left(\phi^{n+1} - \phi^n\right)d\mathbf{x} = \int_{\Omega_i}\Big(&-\Delta t\left[\nabla\cdot(\mathbf{v}\phi^n - \varepsilon\nabla\phi^n)\right. \\ &\left. + \kappa\phi - q\right] + \frac{(\Delta t)^2}{2}\nabla\cdot\left[\mathbf{v}\left(\mathbf{v}\cdot\nabla\phi^n + \kappa\phi - q\right)\right]\Big)d\mathbf{x}. \end{aligned} \tag{13}$$

Then applying the divergence theorem to the spatial terms, a fully explicit characteristic-based scheme for solving Eq. (12) is obtained in the form

$$\begin{aligned} \phi_i^{n+1} &= \phi_i^n - \Delta t\left(\kappa\phi_i^n - q_i^n\right) \\ &\quad - \frac{\Delta t}{|\,\Omega_i\,|}\sum_{j=1}^{N_f}|\,\Gamma_{ij}\,|\,\hat{\mathbf{n}}_{ij}\cdot\Big[\left(\mathbf{v}_{ij}^n\phi_{ij}^n - \varepsilon\nabla\phi_{ij}^n\right) \\ &\quad - \frac{\Delta t}{2}\mathbf{v}_{ij}^n\left(\mathbf{v}_i^n\cdot\nabla\phi_i^n + \kappa\phi_i^n - q_i^n\right)\Big], \end{aligned} \tag{14}$$

where N_f is the number of adjacent cell faces, $|\Omega_i|$ is the measure of Ω_i, Γ_{ij} is the segment of the boundary $\partial\Omega_i$ between the two adjacent control volumes Ω_i and Ω_j, which is defined by

$$\partial\Omega_i = \bigcup_{j=1}^{N_f}\Gamma_{ij} \text{ and } \Gamma_{ij} = \partial\Omega_i \cap \partial\Omega_j, \tag{15}$$

and $|\Gamma_{ij}|$ is the measure of Γ_{ij}. In Eq. (14), the quantities with the subscripts i and ij are evaluated inside the volume Ω_i and at the segment Γ_{ij}, respectively. Further, $\phi_i^n = \phi_i(t^n),\ \phi_{ij}^n = \phi_{ij}(t^n),\ q_i^n = q_i(t^n),\ \mathbf{v}_{ij}^n = \mathbf{v}_{ij}(t^n)$ and $\mathbf{v}_i^n = \mathbf{v}_j(t^n)$. The value of ϕ_i^n is then computed using the volume average

$$\phi_i^n = \frac{1}{|\Omega_i|}\int_{\Omega_i}\phi(\mathbf{x}, t^n)d\mathbf{x}. \tag{16}$$

For the 1-D case of Eq. (14), let $x_{ij} = x_{i\pm\frac{1}{2}}$ for $j = i \pm 1$ and define

$$\nabla\phi_i^n := \frac{\phi_{i+1}^n - \phi_{i-1}^n}{x_{i+1} - x_{i-1}},\ \nabla\phi_{ij}^n := \frac{\phi_j^n - \phi_i^n}{x_j - x_i}. \tag{17}$$

Finally, the scalar quantities at the cell faces, ϕ_{ij}^n, are approximated by applying a Taylor-series expansion in space such that

$$\phi_{ij}^n = \phi_i^n + (\mathbf{x}_{ij} - \mathbf{x}_i)\cdot\nabla\phi_i^n, \tag{18}$$

and for the opposite direction of velocity, the values of ϕ_{ji}^n can be computed from Eq.(19) below, by using the values

from the neighboring volumes according to the upwinding direction,

$$\phi_{ji}^n = \phi_j^n + (\mathbf{x}_{ji} - \mathbf{x}_j) \cdot \nabla \phi_j^n. \tag{19}$$

Finally, the gradient term, $\nabla \phi_{ij}^n$, is approximated by the weighted residuals method which is commonly used in the finite element technique [25]. For the case of triangular control volumes, the stability of a numerical scheme on the triangular grid requires that a Courant-Friedrichs-Lewy (CFL)-like stability criterion must be satisfied. Hence, the time-step within each control volume i for Eq. (14) is determined from [8], [9]

$$\Delta t = C \min_i \left(\frac{\mid \Omega_i \mid}{\max_{j=1,...,N_f} \mid \mathbf{v}_{ij}^n \mid}, \frac{\mid \Gamma_i^c \mid^2}{2\varepsilon} \right), \tag{20}$$

where $\mathbf{v}_{ij}^n$ is the scaled normal velocity at Γ_{ij}, $\mid \Gamma_i^c \mid$ is the characteristic length of cell i and $0 < C \leq 1$.

III. Numerical Results

In this section, numerical simulations obtained using the explicit characteristic-based finite volume method are given for water pollution problems in a reservoir modeled using first a 1-D and then a 2-D ADRE of the form in Eq. (1). In addition, the results obtained for the proposed finite volume method are compared with the results of [1] obtained using the finite difference with implicit FTCS scheme.

A. One dimensional advection-diffusion equation

Using Eq. (1) with a zero reaction term, the 1-D advection-diffusion initial-boundary value problem for water pollutant concentration at the release point of the polluted water can be shown to be [1], [26],

$$\frac{\partial C}{\partial t} + \bar{u}\frac{\partial C}{\partial x} - D_f \frac{\partial^2 C}{\partial x^2} = 0, \quad 0 < x < 1, \ 0 < t \leq 1 \tag{21}$$

with the initial condition

$$C(x,0) = \exp\left(-\frac{(x+0.5)^2}{0.00125} \right), \quad 0 < x < 1, \tag{22}$$

and the boundary conditions

$$C(0,t) = \frac{0.025}{\sqrt{0.000625 + 0.02t}} \exp\left[-\frac{(0.5-t)^2}{(0.00125 + 0.04t)} \right], \quad 0 < t \leq 1, \tag{23}$$

$$C(1,t) = \frac{0.025}{\sqrt{0.000625 + 0.02t}} \exp\left[-\frac{(1.5-t)^2}{(0.00125 + 0.04t)} \right], \quad 0 < t \leq 1. \tag{24}$$

The dependent variable $C(x,t)$ in (21) is the water pollutant concentration (kg/m^3) averaged in depth at longitudinal distance along the stream x at time t, $\bar{u}$ is the water flow velocity in the x-direction and D_f is the dispersion coefficient. From [1], [26], [27] the exact solution of problem (21)-(24) with $\bar{u} = 1$ and $D_f = 0.01$ is

$$C(x,t) = \frac{0.025}{\sqrt{0.000625 + 0.02t}} \exp\left[-\frac{(x+0.5-t)^2}{(0.00125 + 0.04t)} \right]. \tag{25}$$

The graph of the exact solution (25) on the given domain is given in Fig. 1 of [1].

The discrete numerical schemes that were used to solve the 1-D system (21)-(24) were as follows. The spatial domain $0 \leq x \leq 1$ was discretized with $\Delta x = 0.025$ and the time domain $0 \leq t \leq 1$ with $\Delta t = 0.002$. Next, the fully explicit characteristic-based finite volume method of (14) was used with the following values of parameters: $N_f = 3$, $|\Gamma_{ij}| = 1$, $\mathbf{v}_{ij}^n = \bar{u}_{ij} = \bar{u}$, $\mathbf{v}_i^n = \bar{u}_i = \bar{u}$, $\hat{\mathbf{n}}_{ij} = \hat{\mathbf{i}}$ for $j = i \pm 1$. The discretized system for (21)-(24) was then as follows:

$$\begin{aligned} C_i^{n+1} &= C_i^n - \frac{\Delta t}{\mid \Omega_i \mid} \sum_{j=1}^{3} \left(\bar{u}_{ij} C_{ij}^n - D_f \frac{\partial C_{ij}^n}{\partial x} \right) \\ &\quad + \frac{(\Delta t)^2}{2 \mid \Omega_i \mid} \sum_{j=1}^{3} \bar{u}_{ij} \left(\bar{u}_i \frac{\partial C_i^n}{\partial x} \right), \end{aligned} \tag{26}$$

where $i = 0, 1, ..., 40$ and $n = 0, 1, ..., 499$. Finally, substituting the initial and boundary conditions in (22)-(24) into (26) and carrying out the numerical computations, the results shown in Fig.1 were obtained for the water pollutant concentration $C(x,t)$ on the discretized domain.

For the FDM with implicit FTCS, the 1-D scheme of (2) for solving problem (21)-(24) can be written in the form

$$\begin{aligned} &\frac{C_i^{n+1} - C_i^n}{\Delta t} + \bar{u}\frac{C_{i+1}^{n+1} - C_{i-1}^{n+1}}{2\Delta x} \\ &\qquad - D_f \left(\frac{C_{i+1}^{n+1} - 2C_i^{n+1} + C_{i-1}^{n+1}}{(\Delta x)^2} \right) = 0, \end{aligned} \tag{27}$$

where $i = 1, ..., 39$ and $n = 0, 1, ..., 499$ and the diffusion coefficient ε is denoted by D_f. The solution of (27) obtained using the FDM with implicit FTCS with $\Delta x = 0.025, \Delta t = 0.002$ has been given as a 3-D graph in Fig. 2 of [1]. This graph is very similar to Fig. 1.

A comparison of the results for the pollutant concentrations obtained from the exact solution (25) and the numerical schemes in (26) and (27) are shown in Fig. 2 and Table I for $t = 1$ and $0 \leq x \leq 1$. It can be seen that the maximum value of $C(x,1)$ is approximately 0.1741 at $x = 0.5$ for the exact solution and that the numerical simulations are in good agreement with the exact result since the maximum values of $C(x,1)$ obtained using the FVM and FDM are 0.1745 and 0.1688 at $x = 0.5$, respectively. Also, the maximum absolute errors between the numerical and exact solutions at $t = 1$ are 5.38×10^{-3} for the FVM at $x = 0.775$ and 7.24×10^{-3} for the FDM at $x = 0.55$.

A comparison of the exact and numerical values of $C(x,t)$ for $x = 0.5$ and $0 \leq t \leq 1$ are shown in Fig. 3 and Table II. It can be seen that both the FVM and FDM give accurate results in the region $0 \leq t < 0.65$, Then, in the region $0.65 < t < 0.9$, the FDM values are more accurate than the FVM values and, in the region $0.9 < t < 1$, the FVM values are more accurate. From calculus, it was found that the exact solution (25) of $C(0.5,t)$ has the maximum value of 0.1745 at $t = 0.99005$. In comparison, the maximum values of $C(0.5,t)$ obtained from the FVM and the FDM were 0.1745 at $t = 1$ and 0.1688 at $t = 0.996$, respectively. At $x = 0.5$, it was found that the maximum absolute error for the FVM was approximately 6.34×10^{-3} at $t = 0.766$ and the maximum absolute error for the FDM was 7.24×10^{-3} at $t = 0.942$.

From the results in Tables I and II, it can be seen that the numerical results are in good agreement with the exact solution evaluated on the same discretized grid.

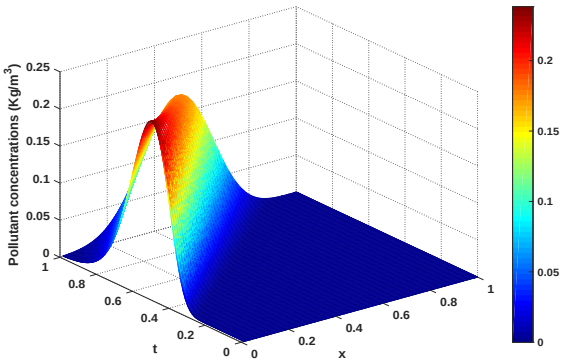

Fig. 1. 3-D graph of the FVM numerical solution of $C(x,t)$ for the initial-boundary value problem of (21) and (22)-(24) for $\Delta x = 0.0250, \Delta t = 0.0020$.

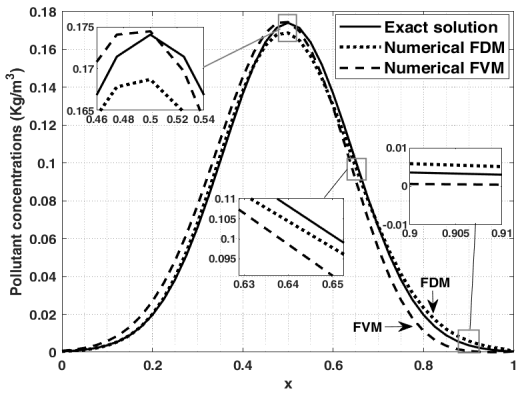

Fig. 2. Comparison of the numerical solutions from FVM and FDM with the exact solution of the test problem (21)-(24) for $t = 1$ for step sizes $\Delta x = 0.0250, \Delta t = 0.0020$.

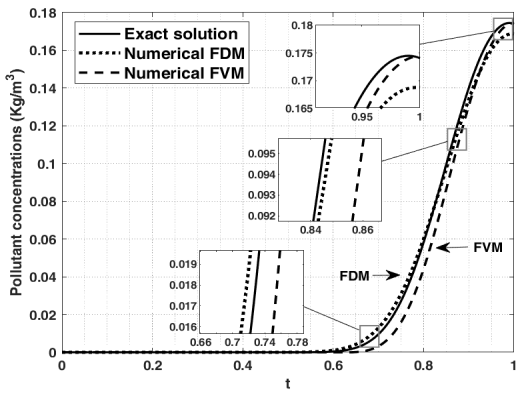

Fig. 3. Comparison of the numerical solutions from FVM and FDM with the exact solution of the test problem (21)-(24) for $x = 0.5$ for step sizes $\Delta x = 0.0250, \Delta t = 0.0020$.

TABLE I
COMPARISON OF NUMERICAL SOLUTIONS OF EQUATIONS (21)-(24) OBTAINED USING THE FVM AND FDM WITH THE EXACT SOLUTION FOR $t = 1$.

$C(x,t)$	Exact	FVM	FDM
$C(0.4,t)$	0.1366	0.1454	0.1381
$C(0.5,t)$	0.1741	0.1745	0.1688
$C(0.6,t)$	0.1366	0.1292	0.1303
$C(0.7,t)$	0.0660	0.0547	0.0666
$C(0.8,t)$	0.0196	0.0112	0.0234
$C(0.9,t)$	0.0036	0.0006	0.0059

TABLE II
COMPARISON OF NUMERICAL SOLUTIONS OF EQUATIONS (21)-(24) OBTAINED USING THE FVM AND FDM WITH THE EXACT SOLUTION FOR $x = 0.5$.

$C(x,t)$	Exact	FVM	FDM
$C(x,0.65)$	0.0024	0.0001	0.0042
$C(x,0.70)$	0.0095	0.0032	0.0129
$C(x,0.75)$	0.0271	0.0159	0.0309
$C(x,0.80)$	0.0582	0.0442	0.0601
$C(x,0.90)$	0.1401	0.1307	0.1340
$C(x,1)$	0.1741	0.1745	0.1688

B. Two dimensional advection-diffusion-reaction model

In this section, numerical results are presented and compared for 2-D advection-diffusion-reaction models for water pollutant concentration in reservoirs with one or two entrance gates and one exit gate.

Using Eq. (1) with a nonzero reaction term, the advection-diffusion-reaction initial-boundary value problem for the water pollutant concentration can be written in the following form [1], [28], [29]:

$$\frac{\partial C}{\partial t} + \bar{u}\frac{\partial C}{\partial x} + \bar{v}\frac{\partial C}{\partial y} - D_f\left(\frac{\partial^2 C}{\partial x^2} + \frac{\partial^2 C}{\partial y^2}\right) + RC = Q(x,y,t), \tag{28}$$

where $C(x,y,t)$ denotes the averaged water pollutant concentration (kg/m^3) at the point $\mathbf{x} = (x,y)$ at time t, $\bar{u}$ and $\bar{v}$ are the average velocity components (m/s) in $x-$ and $y-$directions, respectively, D_f is the pollutant dispersion coefficient (m^2/s), $R \geq 0$ is the decay rate of water pollutant (s^{-1}), and $Q(x,y,t)$ is a source term for the water pollutant concentration (kg/m^3·s). The initial and boundary conditions for the reservoirs will be described in later sections.

In the numerical simulations, it was assumed that the spatial domain was a square with sides of length 2000 m and that the square $0 \leq x, y \leq 2000$ was discretized with $\Delta x = \Delta y = 31.25$. It was also assumed that the time domain in seconds was $0 \leq t \leq 100$ and that it was discretized with $\Delta t = 1$ if the source term Q was a constant and with $\Delta t = 0.01$ if Q was time dependent.

The explicit characteristic-based finite volume scheme for

solving (28) can then be written as follows:

$$C_i^{n+1} = C_i^n - \frac{\Delta t}{\mid \Omega_i \mid} \sum_{j=1}^{3} \Bigg[\left(\bar{u}_{ij} n_x + \bar{v}_{ij} n_y\right) C_{ij}^n - D_f \left(n_x \frac{\partial C_{ij}^n}{\partial x} + n_y \frac{\partial C_{ij}^n}{\partial y} \right) \Bigg] + \frac{(\Delta t)^2}{2 \mid \Omega_i \mid} \sum_{j=1}^{3} \Bigg[\left(\bar{u}_{ij} n_x + \bar{v}_{ij} n_y\right) \left(\bar{u}_i \frac{\partial C_i^n}{\partial x} + \bar{v}_i \frac{\partial C_i^n}{\partial y} \right) + RC_i^n - Q_i^n \Bigg] - \Delta t \left(RC_i^n - Q_i^n \right), \tag{29}$$

where $i = 0, 1, ..., 64$ and $n = 0, 1, ..., 99$.

The implicit FTCS scheme for solving (28) is [1]

$$\frac{C_{i,j}^{n+1} - C_{i,j}^n}{\Delta t} + \bar{u} \frac{C_{i+1,j}^{n+1} - C_{i-1,j}^{n+1}}{2\Delta x} + \bar{v} \frac{C_{i,j+1}^{n+1} - C_{i,j-1}^{n+1}}{2\Delta y} - D_f \left[\frac{C_{i+1,j}^{n+1} - 2C_{i,j}^{n+1} + C_{i-1,j}^{n+1}}{(\Delta x)^2} + \frac{C_{i,j+1}^{n+1} - 2C_{i,j}^{n+1} + C_{i,j-1}^{n+1}}{(\Delta y)^2} \right] + RC_{i,j}^{n+1} = Q_{i,j}^n, \tag{30}$$

where $i, j = 1, ..., 63$ and $n = 0, 1, ..., 99$.

In the numerical simulations, the water pollutant concentrations $C(x, y, t)$ were computed for changes in the number of entrance gates in the reservoir, changes in the values of the diffusion coefficient D_f and changes in the values of the source terms $Q(x, y, t)$. The values of the parameters that were used in the simulations are listed in Table III [1], [29].

TABLE III
VALUES OF PARAMETERS

Parameter	Definition	Value	Units
$\bar{u}$	Average u velocity	-0.002461	m$\cdot$ s^{-1}
$\bar{v}$	Average v velocity	0.04527	m$\cdot$ s^{-1}
R	Decay rate	10^{-7}	s^{-1}
D_f	Dispersion coeffs.	50, 200	m$^2\cdot$ s^{-1}
$Q(x, y, t)$	Source terms	$0, -0.01, -e^{-t}$	kg$\cdot$ m$^{-3}\cdot$ s^{-1}

1) Reservoir with one entrance gate: The first model considered was the reservoir with one entrance gate and one exit gate shown in Fig. 4.

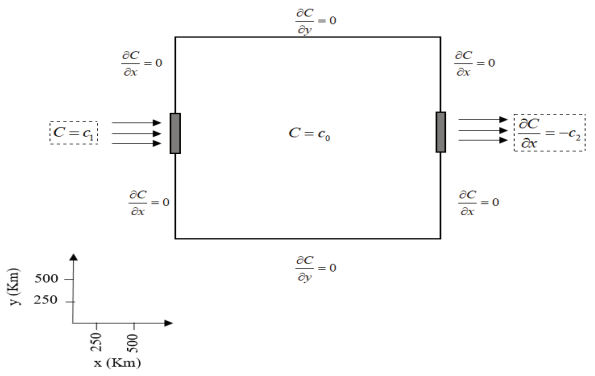

Fig. 4. The initial and boundary conditions for the reservoir with one entrance gate and one exit gate.

It was assumed that the initial conditions for the numerical simulations were

$$C(x, y, 0) = c_0 \ ; \ 0 \le x \le 2000, \ 0 \le y \le 2000, \tag{31}$$

and that the boundary conditions were

$$\begin{aligned} &C(0, y, t) = c_1 \ ; \ 843.75 \le y \le 1156.25, \\ &\frac{\partial C}{\partial x}(0, y, t) = 0 \ ; \ 0 \le y < 843.75 \text{ and } 1156.25 < y \le 2000, \\ &\frac{\partial C}{\partial x}(2000, y, t) = -c_2 \ ; \ 843.75 \le y \le 1156.25, \\ &\frac{\partial C}{\partial x}(2000, y, t) = 0 \ ; \ 0 \le y < 843.75 \text{ and } 1156.25 < y \le 2000, \\ &\frac{\partial C}{\partial y}(x, 0, t) = 0 \ ; \ 0 < x < 2000, \\ &\frac{\partial C}{\partial y}(x, 2000, t) = 0 \ ; \ 0 < x < 2000, \end{aligned} \tag{32}$$

where the initial concentration in the reservoir was $c_0 = 1.5$ kg/m^3, the concentration at the entrance gate was $c_1 = 10$ kg/m^3 and the concentration flow rate at the exit gate was $c_2 = -0.001$ kg/m^4.

Applying the schemes (29) and (30) to the problem consisting of equation (28) and conditions (31) and (32), numerical results were obtained for the three different functions for the source terms $Q(x, y, t)$ and the parameter values listed in Table III.

(a) $\mathbf{Q(x, y, t) = 0}$: Fig. 5 shows a comparison of the 2-D graphs obtained from the FVM and FDM for the distribution of the water pollutant concentration $C(x, y, t)$ at $y = 1000$ m and the final time $t = 100$ s. In particular, Fig. 5 (a) shows the results for the dispersion coefficient $D_f = 50$ and Fig. 5 (b) shows the results for $D_f = 200$. It can be seen that the value of $C(x, y, t)$ has reduced from its value of 10 (kg/m^3) at the entrance gate to the initial concentration in the reservoir of 1.5 (kg/m^3) after $x = 300$ m for $D_f = 50$ and after $x = 600$ m for $D_f = 200$. It can also be seen that $C(x, y, t)$ eventually decreases to 1.4243 (kg/m^3) at the exit gate for $D_f = 50$ and to 1.3606 (kg/m^3) for $D_f = 200$. The numerical values of $C(x, y, t)$ for $D_f = 50$ and $D_f = 200$ are shown in Table IV for a range of values of x.

(b) $\mathbf{Q(x, y, t) = -0.01}$: Fig. 6 shows a comparison of the 2-D graphs obtained from the FVM and FDM for the distribution of the water pollutant concentration $C(x, y, t)$ at $y = 1000$ m and the final time $t = 100$ s. In particular, Fig. 6 (a) shows the results for the dispersion coefficient $D_f = 50$ and Fig. 6 (b) shows the results for $D_f = 200$. It can be seen that the value of $C(x, y, t)$ has reduced from its value of 10 (kg/m^3) at the entrance gate to the initial concentration in the reservoir of 0.5 (kg/m^3) after $x = 400$ m for $D_f = 50$ and after $x = 600$ m for $D_f = 200$. It can also be seen that $C(x, y, t)$ eventually decreases to 0.4243 (kg/m^3) at the exit gate for $D_f = 50$ and to 0.3606 (kg/m^3) for $D_f = 200$. The numerical values of $C(x, y, t)$ for $D_f = 50$ and $D_f = 200$ are shown in Table V for a range of values of x.

(c) $\mathbf{Q(x, y, t) = -e^{-t}}$: Fig. 7 shows a comparison of the 2-D graphs obtained from the FVM and FDM for the

distribution of the water pollutant concentration $C(x, y, t)$ at $y = 1000$ m and the final time $t = 100$ s. In particular, Fig. 7 (a) shows the results for the dispersion coefficient $D_f = 50$ and Fig. 7 (b) shows the results for $D_f = 200$. It can be seen that the value of $C(x, y, t)$ has reduced from its value of 10 (kg/m^3) at the entrance gate to the initial concentration in the reservoir of 0.5 (kg/m^3) after $x = 350$ m for $D_f = 50$ and after $x = 600$ m for $D_f = 200$. It can also be seen that $C(x, y, t)$ eventually decreases to 0.4248 (kg/m^3) at the exit gate for $D_f = 50$ and to 0.3609 (kg/m^3) for $D_f = 200$. The numerical values of $C(x, y, t)$ for $D_f = 50$ and $D_f = 200$ are shown in Table VI for a range of values of x.

From the above numerical results, it can be seen that the values computed from the FVM and FDM are in good agreement for all cases. It can also be seen that the higher value of the diffusion coefficient $D_f = 200$ gives a more gradual change in the concentration $C(x, y, t)$ than the lower value $D_f = 50$ for the same value of the source term Q.

An example of the the 3-D distribution of the water pollutant concentration $C(x, y, t)$ and its contour at $t = 100$ s obtained using the FVM is shown in Fig. 8 for $Q(x, y, t) = -0.01$ and $D_f = 200$.

TABLE IV
NUMERICAL SOLUTIONS OF THE PROBLEM CONSISTING OF (28), (31) AND (32) FOR THE ONE ENTRANCE GATE RESERVOIR FOR $Q = 0$ AT $y = 1000$, $t = 100$.

$C(x, y, t)$	$D_f = 50$		$D_f = 200$	
	FVM	FDM	FVM	FDM
$C(0, y, t)$	10	10	10	10
$C(125, y, t)$	3.2580	3.2416	5.4336	5.4883
$C(250, y, t)$	1.6026	1.6164	2.8848	2.9198
$C(500, y, t)$	1.4999	1.5000	1.5714	1.5784
$C(1000, y, t)$	1.4999	1.4999	1.4999	1.4999
$C(1750, y, t)$	1.4996	1.4992	1.4848	1.4827
$C(1875, y, t)$	1.4893	1.4864	1.4465	1.4422
$C(2000, y, t)$	1.4243	1.4048	1.3606	1.3450

TABLE V
NUMERICAL SOLUTIONS OF THE PROBLEM CONSISTING OF (28), (31) AND (32) FOR THE ONE ENTRANCE GATE RESERVOIR FOR $Q = -0.01$ AT $y = 1000$, $t = 100$.

$C(x, y, t)$	$D_f = 50$		$D_f = 200$	
	FVM	FDM	FVM	FDM
$C(0, y, t)$	10	10	10	10
$C(125, y, t)$	2.3398	2.3294	4.7309	4.7924
$C(250, y, t)$	0.6047	0.6196	1.9529	1.9919
$C(500, y, t)$	0.4999	0.5000	0.5730	0.5805
$C(1000, y, t)$	0.4999	0.4999	0.4999	0.4999
$C(1750, y, t)$	0.4996	0.4992	0.4848	0.4827
$C(1875, y, t)$	0.4893	0.4864	0.4465	0.4422
$C(2000, y, t)$	0.4243	0.4048	0.3606	0.3450

2) Reservoir with two entrance gates: In this section, the problem of water pollutant dispersion in the reservoir with two entrance gates and one exit gate shown in Fig. 9 is discussed. Numerical solutions of the water pollutant dispersion problem in the reservoir were obtained for the

TABLE VI
NUMERICAL SOLUTIONS OF THE PROBLEM CONSISTING OF (28), (31) AND (32) FOR THE ONE ENTRANCE GATE RESERVOIR FOR $Q = -e^{-t}$ AT $y = 1000$, $t = 100$.

$C(x, y, t)$	$D_f = 50$		$D_f = 200$	
	FVM	FDM	FVM	FDM
$C(0, y, t)$	10	10	10	10
$C(125, y, t)$	2.4371	2.4563	4.8889	4.9689
$C(250, y, t)$	0.6278	0.6322	2.0426	2.0961
$C(500, y, t)$	0.4998	0.5050	0.5821	0.5906
$C(1000, y, t)$	0.4997	0.5049	0.4999	0.5049
$C(1750, y, t)$	0.4993	0.5043	0.4848	0.4877
$C(1875, y, t)$	0.4890	0.4914	0.4467	0.4471
$C(2000, y, t)$	0.4248	0.4097	0.3609	0.3498

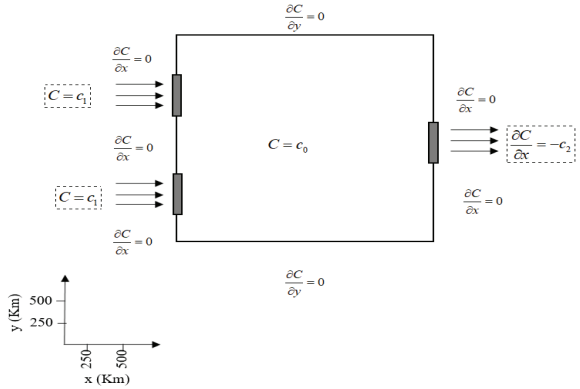

Fig. 9. The initial and boundary conditions for the reservoir with two entrance gates and one exit gate.

governing equation (28) with the initial conditions in (31) and the boundary conditions in (33).

$$
\begin{aligned}
&C(0, y, t) = c_1 \ ; \ 437.5 \le y \le 562.5 \text{ and} \\
&\qquad 1437.5 \le y \le 1562.5, \\
&\frac{\partial C}{\partial x}(0, y, t) = 0 \ ; \ 0 \le y < 437.5, \ 562.5 < y < 1437.5 \\
&\qquad \text{and } 1562.5 < y \le 2000, \\
&\frac{\partial C}{\partial x}(2000, y, t) = -c_2 \ ; \ 843.75 \le y \le 1156.25, \\
&\frac{\partial C}{\partial x}(2000, y, t) = 0 \ ; \ 0 \le y < 843.75 \text{ and} \\
&\qquad 1156.25 < y \le 2000, \\
&\frac{\partial C}{\partial y}(x, 0, t) = 0 \ ; \ 0 < x < 2000, \\
&\frac{\partial C}{\partial y}(x, 2000, t) = 0 \ ; \ 0 < x < 2000. \qquad (33)
\end{aligned}
$$

Applying the FVM in (29) and the FDM in (30), numerical results were computed for the reservoir for the parameter values and the three values for the source term $Q(x, y, t)$ given in Table III.

(a) $\mathbf{Q(x, y, t) = 0}$: Figs. 10 (a)-(b) show plots of the water pollutant concentration $C(x, y, t)$ at the final time $t = 100$ s at the midpoint of the first gate ($y = 500$ m) for $D_f = 50$ and $D_f = 200$, respectively. As in the one entrance gate case, it can be seen that the concentration of $C(x, y, t)$ of 10 (kg/m^3) at an entrance gate has reduced faster to the initial concentration in the reservoir of 1.5 (kg/m^3) for $D_f = 50$

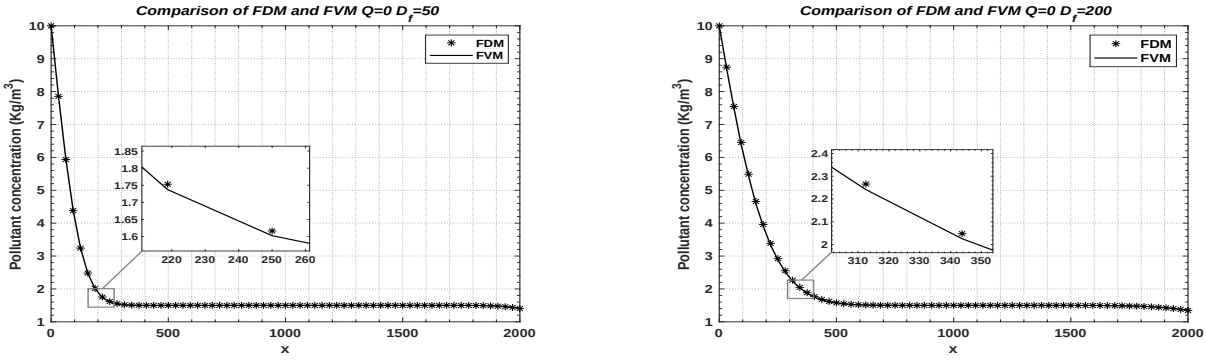

(a) (b)

Fig. 5. Numerical comparisons of the problem consisting of (28), (31) and (32) for the one entrance gate reservoir using the FVM (solid line) and FDM (asterisk) for $Q = 0$ and $y = 1000$, $t = 100$, $\Delta t = 1$: (a) $D_f = 50$, (b) $D_f = 200$.

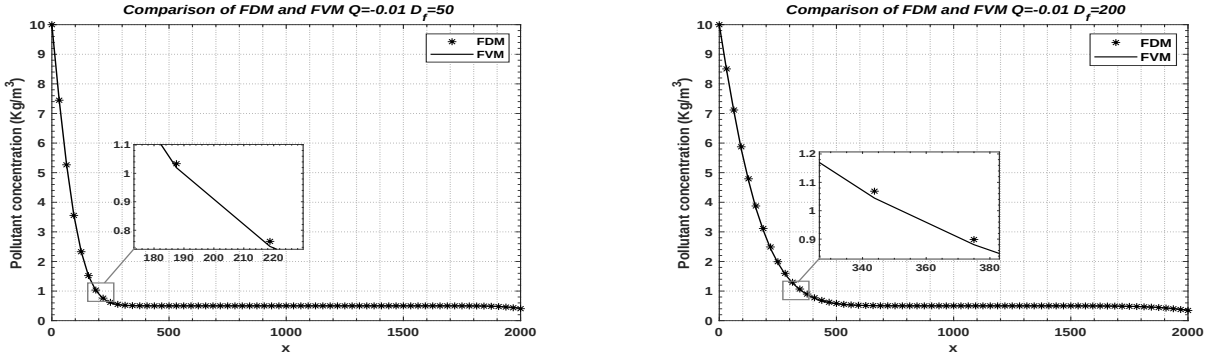

(a) (b)

Fig. 6. Numerical comparisons of the problem consisting of (28), (31) and (32) for the one entrance gate reservoir using the FVM (solid line) and FDM (asterisk) for $Q = -0.01$ and $y = 1000$, $t = 100$, $\Delta t = 1$: (a) $D_f = 50$, (b) $D_f = 200$.

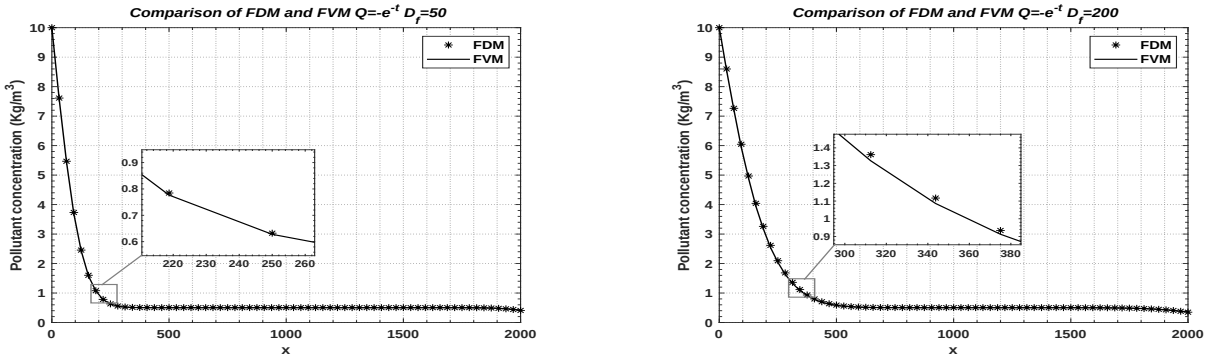

(a) (b)

Fig. 7. Numerical comparisons of the problem consisting of (28), (31) and (32) for the one entrance gate reservoir using the FVM (solid line) and FDM (asterisk) for $Q = -e^{-t}$ and $y = 1000$, $t = 100$, $\Delta t = 0.01$: (a) $D_f = 50$, (b) $D_f = 200$.

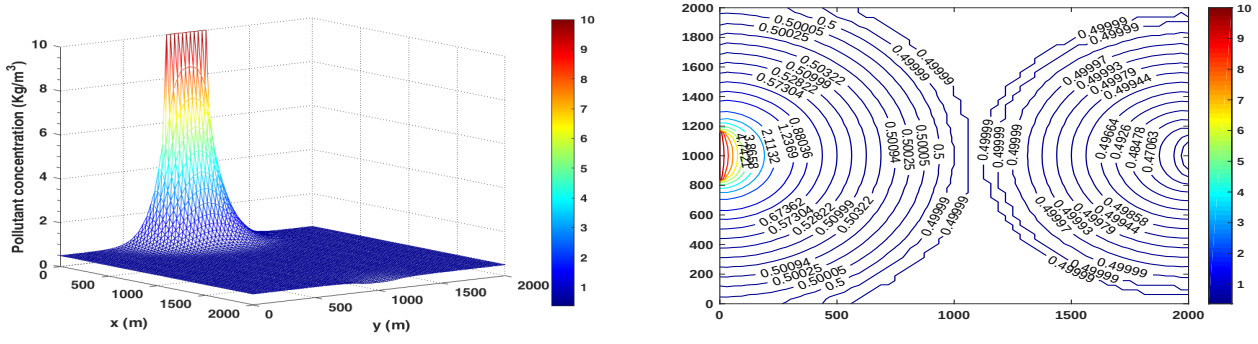

(a) (b)

Fig. 8. Numerical solutions of the water pollutant concentration $C(x, y, t)$ for the one entrance gate reservoir evaluated at $t = 100$ using the FVM for $Q(x, y, t) = -0.01$ and $D_f = 200$: (a) 3-D graph, (b) contour graph.

than for $D_f = 200$. Further, there is very good agreement between the FVM and FDM results.

Figs. 10 (c)-(d) show plots of $C(x, y, t)$ at $t = 100$ s at the midpoint of the reservoir's vertical side ($y = 1000$ m) for $D_f = 50$ and $D_f = 200$, respectively. For $D_f = 50$, there is good agreement between the FVM and FDM results with the initial concentration $C(x, 1000, t)$ at $x = 0$ being equal to the initial concentration in the reservoir of 1.5 (kg/m^3) before it begins to decay at approximately $x = 1800$ m to a final concentration of 1.4243 (kg/m^3) at the exit gate. However, for $D_f = 200$ there are appreciable differences between the FVM and FDM results near the midpoint of the entrance gate at $x = 0$ and the exit gate at $x = 2000$. For the FVM, the concentration is 1.6133 (kg/m^3) at $x = 0, y = 1000$ and 1.3606 (kg/m^3) at $x = 2000, y = 1000$ compared with 1.5875 (kg/m^3) and 1.3450 (kg/m^3) for the FDM.

Since the reservoir has two symmetric entrance gates, the numerical results will be symmetric about $y = 1000$ m.

The values of the concentration $C(x, y, t)$ at different values of x for $y = 1000$ m and $t = 100$ s are shown in Table VII.

Figs. 11 (a) and (b) show the concentrations at $x = 0$ for $t = 100$ s for $D_f = 50$ and $D_f = 200$, respectively. It can be seen that the FVM and FDM results are in quite good agreement, but with the FVM concentrations being slightly higher than the FDM concentrations. Figs. 11 (c) and (d) show the concentrations at $x = 2000$ m for $t = 100$ s for $D_f = 50$ and $D_f = 200$, respectively. In both cases, the results for the FVM and FDM show large differences near the center of the exit gate with the FVM giving appreciably higher values than the FDM.

(b) $\mathbf{Q(x, y, t) = -0.01}$: The results for this case are shown in Figs. 12 (a)-(d) and Figs. 13 (a)-(d). In general, it can be seen that the patterns are the same as for the $Q(x, y, t) = 0$ case, but with some differences in detail. In particular, the initial concentration in the reservoir is 0.5 (kg/m^3) in this case compared with 1.5 (kg/m^3) for case (a). The values of the concentration $C(x, y, t)$ at different values of x for $y = 1000$ m and $t = 100$ s are shown in Table VIII.

(c) $\mathbf{Q(x, y, t) = -e^{-t}}$: The results for this case are shown in Figs. 14 (a)-(d) and Figs. 15 (a)-(d). It can again be seen that the patterns are the same as for the $Q(x, y, t) = 0$ and $Q(x, y, t) = -0.01$ cases, but with some differences in detail. In particular, there is a much larger difference between the FVM and FDM concentrations at the midpoint of the entrance gates ($y = 1000$ m) in Fig. 14 (c) than in Figs 10 (c) and 12 (c). There is also a much larger difference between the FVM and FDM concentrations at $x = 2000$ m in Figs. 15 (c) and (d) than in Figs 11 (c) and (d) and 13 (c) and (d). The values of the concentration $C(x, y, t)$ at different values of x for $y = 1000$ m and $t = 100$ s are shown in Table IX.

An example of the 3-D distribution of the water pollutant concentration $C(x, y, t)$ and its contour at $t = 100$ s obtained using the FVM for the two entrance gates reservoir is shown in Fig. 16 for $Q(x, y, t) = -e^{-t}$ and $D_f = 200$.

The FVM and FDM were used to compute the changes in the pollutant concentration as a function of time at the center of an entrance gate for the one entrance gate reservoir for $D_f = 50$ and $D_f = 200$ for three different values of $Q(x, y, t)$. Comparisons of the results for the FVM and FDM at $x = 250$ m and $y = 1000$ m are shown in Fig. 17 (a) for $D_f = 50$ and in Fig. 18 (a) for $D_f = 200$. It can be seen that there is good agreement between the FVM and FDM concentrations in all cases. It can also be seen that there are big differences between the three $Q(x, y, t)$ cases for both $D_f = 50$ and $D_f = 200$. For $D_f = 50$, the concentration is constant for most of the time for the $Q = 0$ case, but with a very slow increase near $t = 100$ s. For the $Q = -0.01$ case, there is a linear decrease in concentration with time. Finally, for the $Q = -e^{-t}$ case, there is an initial rapid decrease in concentration followed by a very slow increase with time. For $D_f = 200$, the concentration steadily increases with time, for the $Q = -0.01$ case the concentration first decreases slowly and then increases slowly, and, finally, for the $Q = -e^{-t}$ case there is initially a rapid decrease followed by a steady increase at a similar rate to the $Q = 0$ case.

The FVM and FDM were also used to compute the changes in the pollutant concentration as a function of time at the midpoint between the two gates of the two entrance gate reservoir for $D_f = 50$ and $D_f = 200$ for three different values of $Q(x, y, t)$. Comparisons of the results for the FVM and FDM at $x = 250$ m and $y = 1000$ m are shown in Fig.17 (b) for $D_f = 50$ and in Fig.18 (b) for $D_f = 200$. It can be seen that there is again good agreement between the FVM and FDM concentrations in all cases and there are again big differences between the three $Q(x, y, t)$ cases for both $D_f = 50$ and $D_f = 200$. A comparison of the results for $D_f = 50$ in Figs. 17 (a) and (b) shows that the behavior for different Q values are similar for the center of one entrance gate and the midpoint of two entrance gates. However, a comparison of the results for $D_f = 200$ in Figs. 18 (a) and (b) shows that the behavior for the three Q cases are different for the two reservoirs. In fact, the results in Fig. 18 (b) show similar behavior for the three Q cases with the behavior in Figs. 17 (a) and (b) for $D_f = 50$.

TABLE VII
NUMERICAL SOLUTIONS OF THE PROBLEM CONSISTING OF (28), (31) AND (33) FOR THE TWO ENTRANCE GATES RESERVIOR FOR $Q = 0$ AT $y = 1000$, $t = 100$.

$C(x, y, t)$	$D_f = 50$		$D_f = 200$	
	FVM	FDM	FVM	FDM
$C(0, y, t)$	1.5000	1.5000	1.6133	1.5875
$C(125, y, t)$	1.5000	1.5000	1.5893	1.5732
$C(250, y, t)$	1.4999	1.4999	1.5446	1.5386
$C(500, y, t)$	1.4999	1.4999	1.5020	1.5032
$C(1000, y, t)$	1.4999	1.4999	1.4999	1.4999
$C(1750, y, t)$	1.4996	1.4992	1.4848	1.4827
$C(1875, y, t)$	1.4893	1.4864	1.4465	1.4422
$C(2000, y, t)$	1.4243	1.4048	1.3606	1.3450

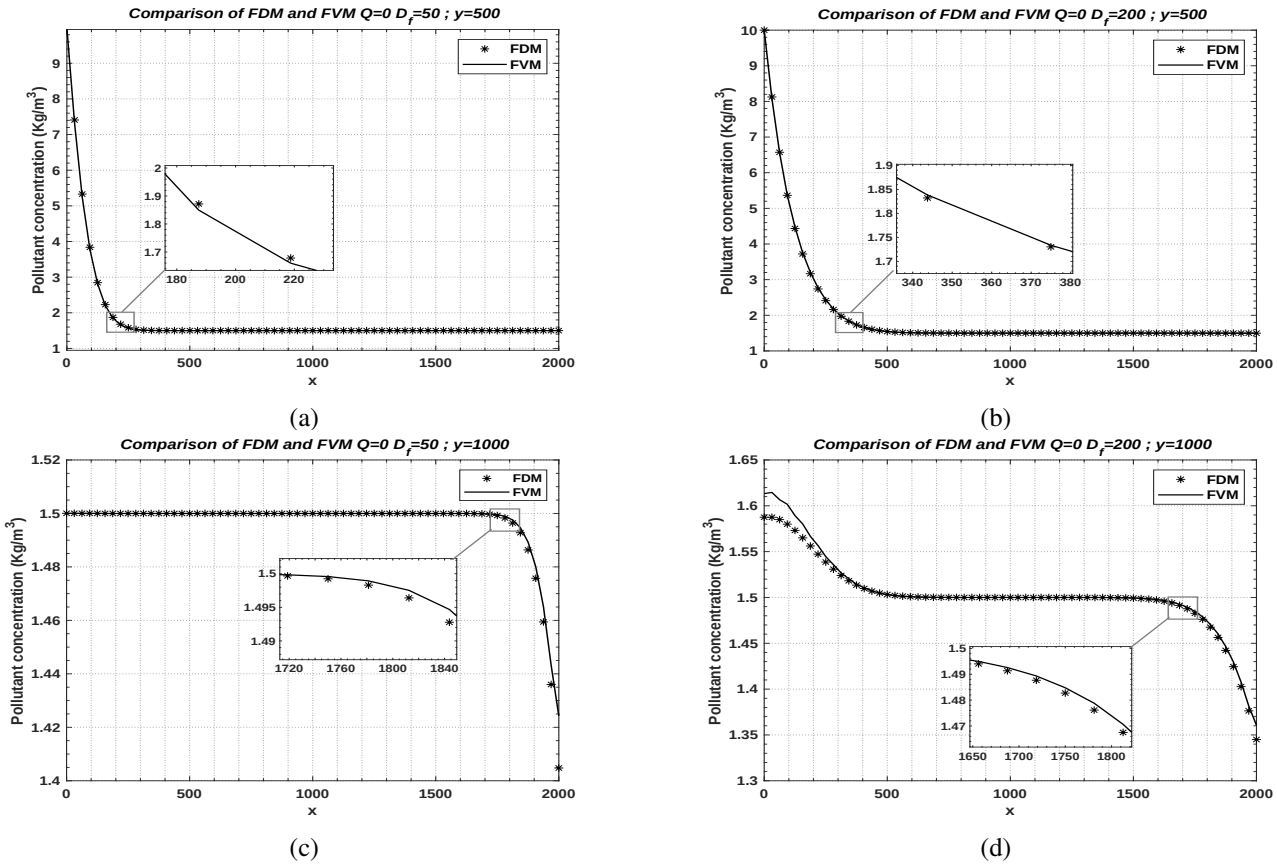

Fig. 10. Numerical comparisons of the problem consisting of (28), (31) and (33) for the two entrance gates reservoir using the FVM and FDM for $Q = 0$ and $t = 100$, $\Delta t = 1$, $y = 500$: (a) $D_f = 50$, (b) $D_f = 200$ and $y = 1000$: (c) $D_f = 50$, (d) $D_f = 200$.

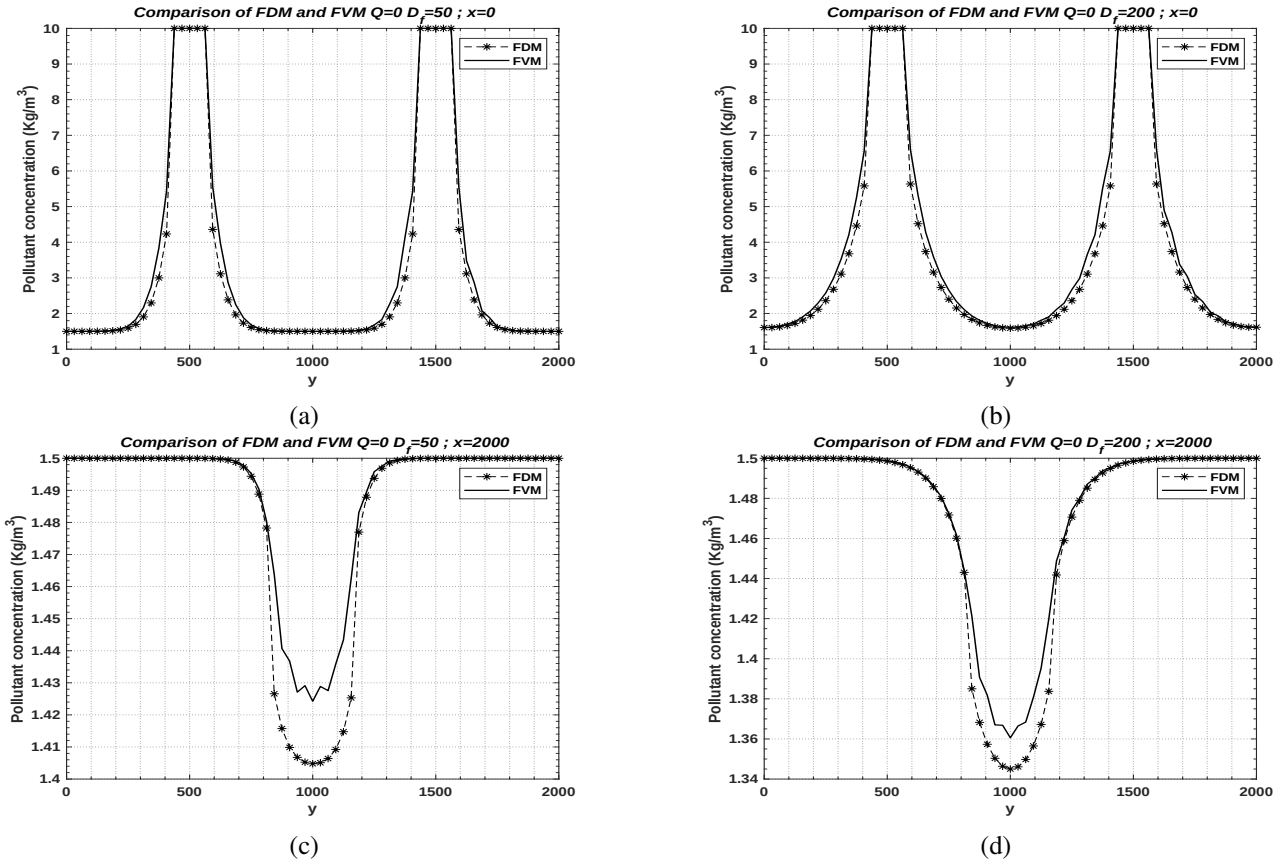

Fig. 11. Numerical comparisons of the problem consisting of (28), (31) and (33) for the two entrance gates reservoir using the FVM and FDM when $Q = 0$ and $t = 100$, $\Delta t = 1$, $x = 0$: (a) $D_f = 50$, (b) $D_f = 200$ and $x = 2000$: (c) $D_f = 50$, (d) $D_f = 200$.

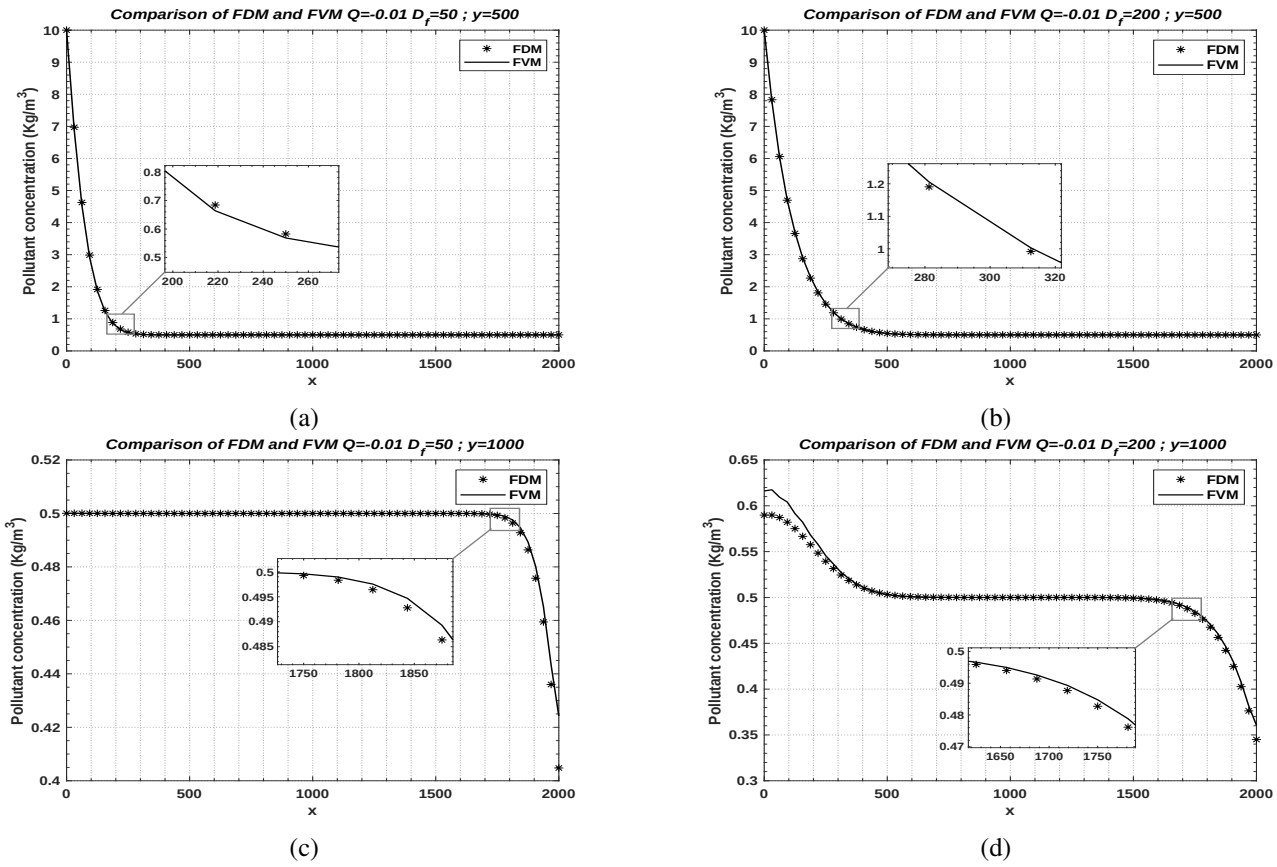

Fig. 12. Numerical comparisons of the problem consisting of (28), (31) and (33) for the two entrance gates reservoir using the FVM and FDM when $Q = -0.01$ and $t = 100$, $\Delta t = 1$, $y = 500$: (a) $D_f = 50$, (b) $D_f = 200$ and $y = 1000$: (c) $D_f = 50$, (d) $D_f = 200$.

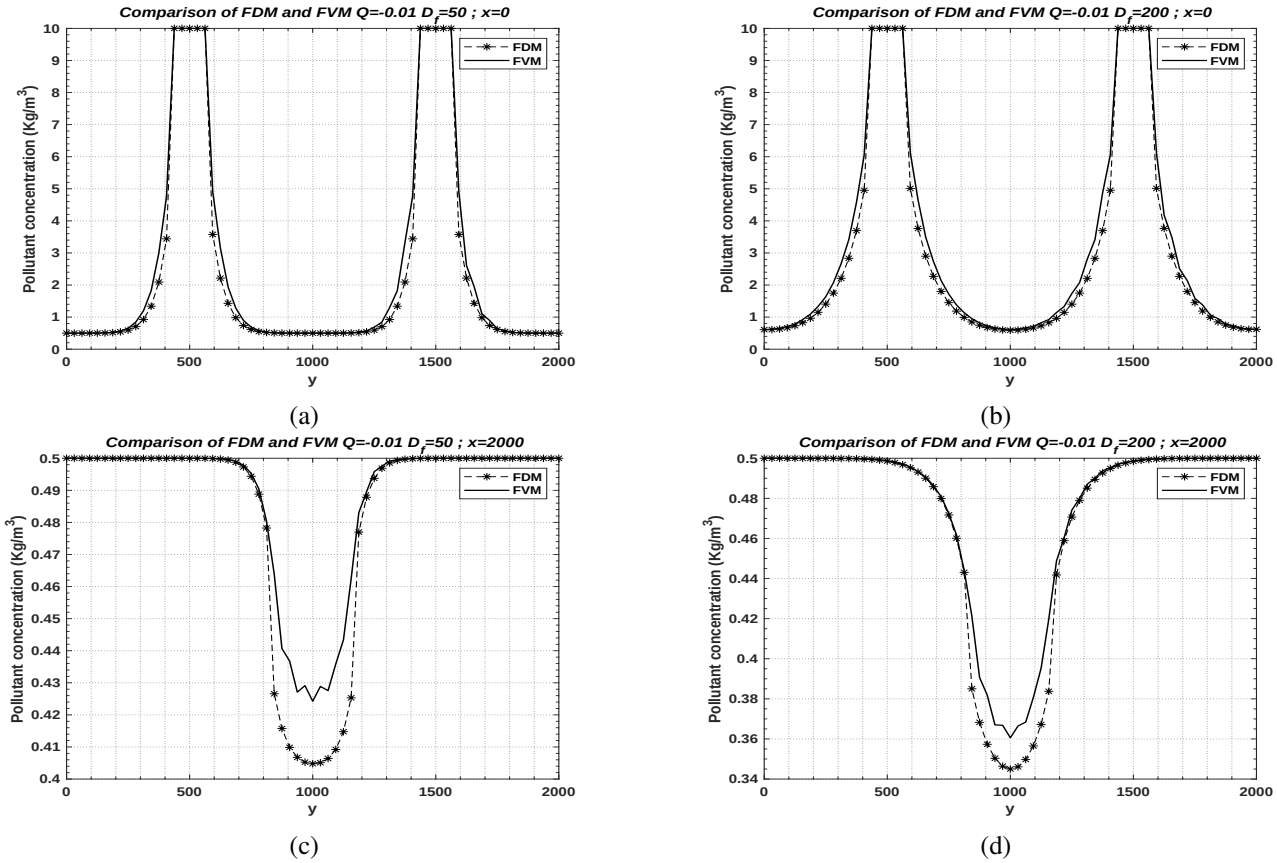

Fig. 13. Numerical comparisons of the problem consisting of (28), (31) and (33) for the two entrance gates reservoir using the FVM and FDM when $Q = -0.01$ and $t = 100$, $\Delta t = 1$, $x = 0$: (a) $D_f = 50$, (b) $D_f = 200$ and $x = 2000$: (c) $D_f = 50$, (d) $D_f = 200$.

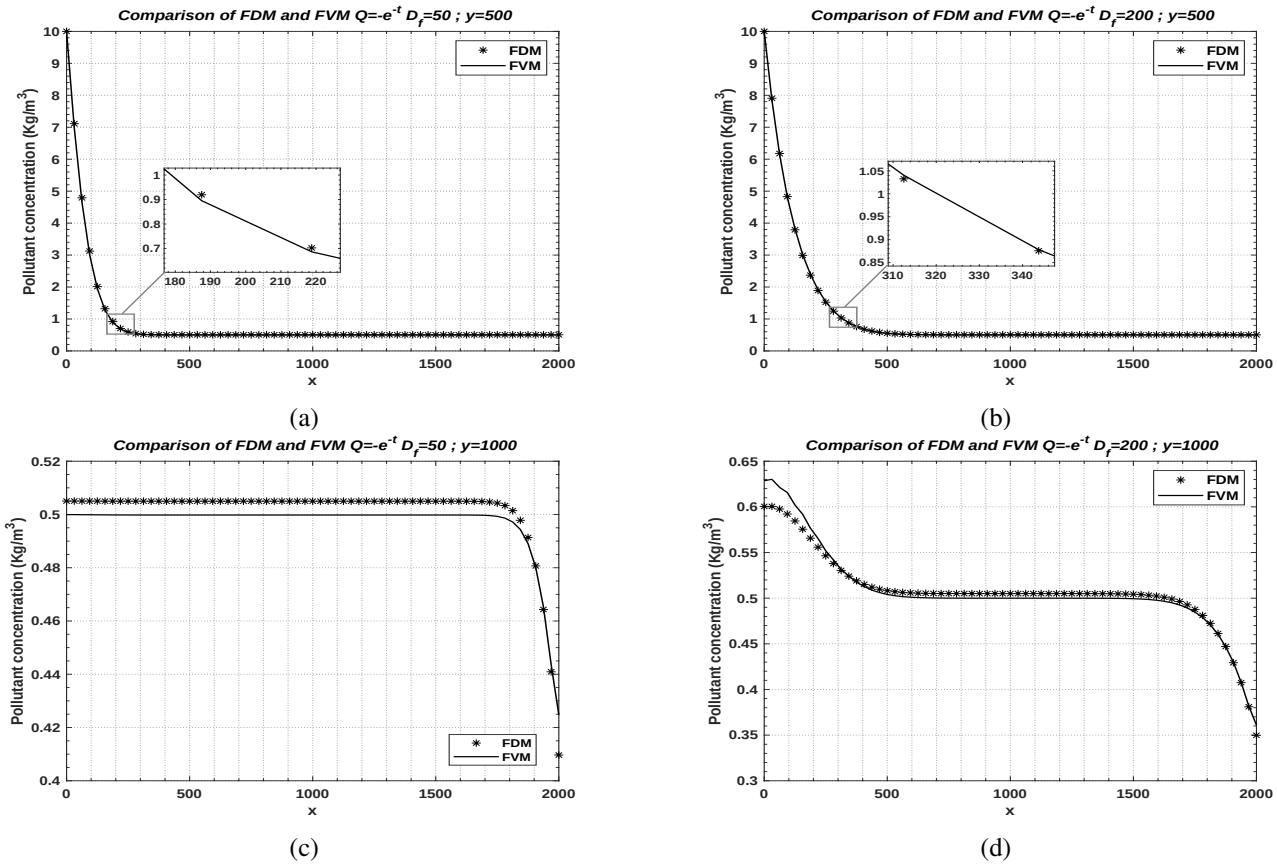

Fig. 14. Numerical comparisons of the problem consisting of (28), (31) and (33) for the two entrance gates reservoir using the FVM and FDM when $Q = -e^{-t}$ and $t = 100$, $\Delta t = 0.01$, $y = 500$: (a) $D_f = 50$, (b) $D_f = 200$ and $y = 1000$: (c) $D_f = 50$, (d) $D_f = 200$.

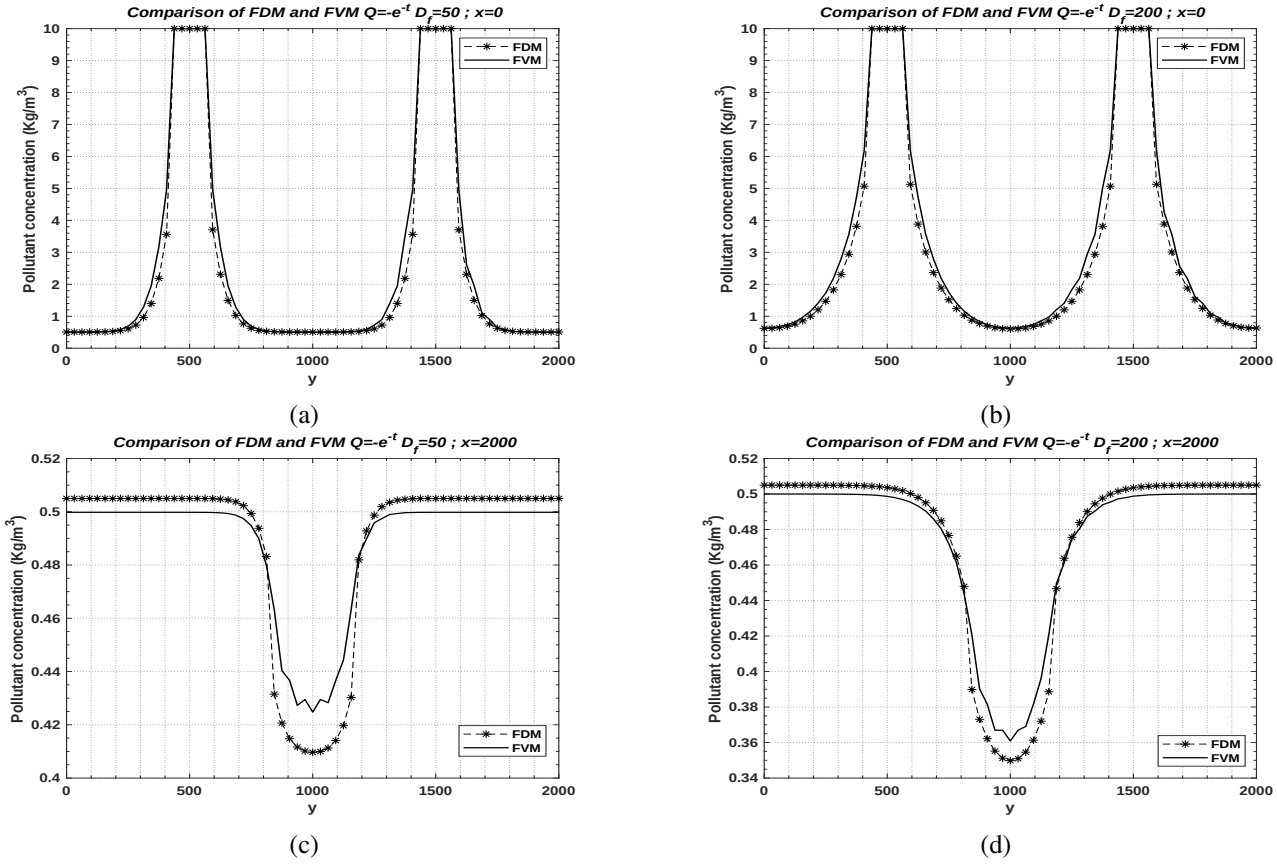

Fig. 15. Numerical comparisons of the problem consisting of (28), (31) and (33) for the two entrance gates reservoir using the FVM and FDM when $Q = -e^{-t}$ and $t = 100$, $\Delta t = 0.01$, $x = 0$: (a) $D_f = 50$, (b) $D_f = 200$ and $x = 2000$: (c) $D_f = 50$, (d) $D_f = 200$.

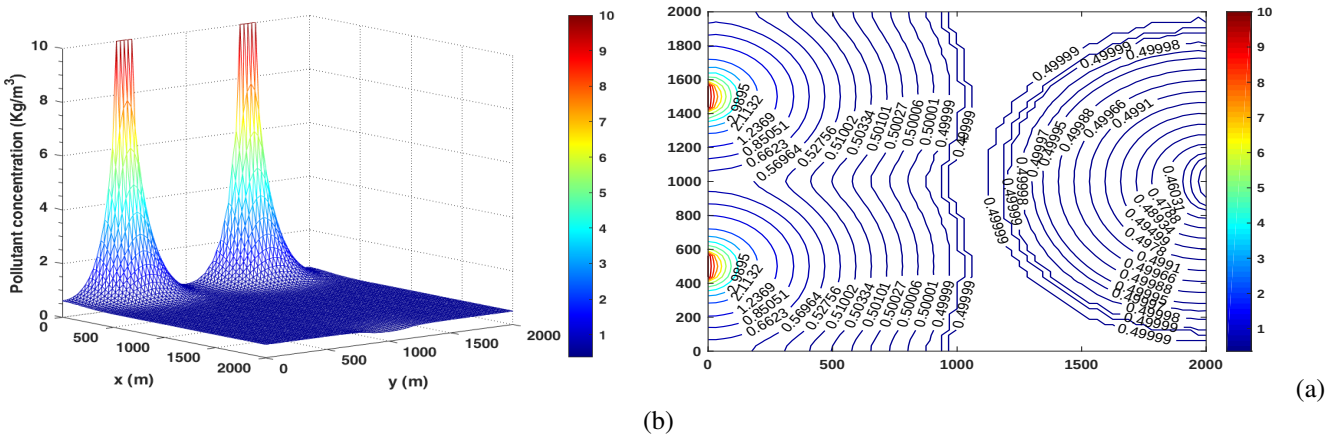

Fig. 16. Numerical plots of the water pollutant concentration $C(x, y, t)$ for the two entrance gates reservoir at $t = 100$ using the FVM for $Q(x, y, t) = -0.01$ and $D_f = 200$: (a) 3-D graph, (b) contour graph.

TABLE VIII
NUMERICAL SOLUTIONS OF THE PROBLEM CONSISTING OF (28), (31) AND (33) FOR THE TWO ENTRANCE GATES RESERVIOR FOR $Q = -0.01$ AT $y = 1000$, $t = 100$.

$C(x, y, t)$	$D_f = 50$		$D_f = 200$	
	FVM	FDM	FVM	FDM
$C(0, y, t)$	0.5000	0.5001	0.6162	0.5899
$C(125, y, t)$	0.5000	0.5000	0.5915	0.5751
$C(250, y, t)$	0.4999	0.4999	0.5455	0.5395
$C(500, y, t)$	0.4999	0.4999	0.5032	0.5033
$C(1000, y, t)$	0.4999	0.4999	0.4999	0.4999
$C(1750, y, t)$	0.4996	0.4992	0.4848	0.4827
$C(1875, y, t)$	0.4893	0.4864	0.4465	0.4422
$C(2000, y, t)$	0.4243	0.4048	0.3606	0.3450

TABLE IX
NUMERICAL SOLUTIONS OF THE PROBLEM CONSISTING OF (28), (31) AND (33) FOR THE TWO ENTRANCE GATES RESERVIOR FOR $Q = -e^{-t}$ AT $y = 1000$, $t = 100$.

$C(x, y, t)$	$D_f = 50$		$D_f = 200$	
	FVM	FDM	FVM	FDM
$C(0, y, t)$	0.4999	0.5050	0.6286	0.6005
$C(125, y, t)$	0.4999	0.5050	0.6020	0.5846
$C(250, y, t)$	0.4998	0.5050	0.5518	0.5464
$C(500, y, t)$	0.4998	0.5050	0.5040	0.5082
$C(1000, y, t)$	0.4998	0.5050	0.5000	0.5050
$C(1750, y, t)$	0.4993	0.5043	0.4848	0.4877
$C(1875, y, t)$	0.4890	0.4914	0.4467	0.4471
$C(2000, y, t)$	0.4248	0.4097	0.3609	0.3498

IV. CONCLUSION

An explicit characteristic-based finite volume method (FVM) has been applied to obtain numerical solutions for advection-diffusion-reaction equations (ADREs). The method has been applied to solve 1-D and 2-D water pollution problems which can be modeled in terms of ADREs. The FVM results have been compared with numerical results obtained using a finite difference method (FDM) with implicit forward time central space (FTCS) scheme [1]. For the 1-D ADRE, numerical solutions from the two methods have also been compared with the exact solution. The results show that, in general, the FVM and FDM errors were of similar magnitude for the step sizes used. For the 2-D case, detailed numerical simulations have been carried out for square reservoirs with either one or two entrance gates and one exit gate for polluted water for high and low values of the diffusion coefficient and for three representative source terms. The results show that, in general, the FVM and FDM results were in good agreement except for some appreciable differences in the calculated concentrations near the entrance and exit gates.

REFERENCES

[1] K. Pananu, S. Sungnul, S. Sirisubtawee, and S. Phongthanapanich, "Convergence and applications of the implicit finite difference method for advection-diffusion-reaction equations." *IAENG International Journal of Computer Science*, vol. 47, no. 4, pp. 645–663, 2020.

[2] G. Gurarslan, H. Karahan, D. Alkaya, M. Sari, and M. Yasar, "Numerical solution of advection-diffusion equation using a sixth-order compact finite difference method," *Mathematical Problems in Engineering*, vol. 2013, 2013.

[3] W. Qin, D. Ding, and X. Ding, "A non-standard finite difference scheme for an advection-diffusion-reaction equation," *Mathematical Methods in the Applied Sciences*, vol. 38, no. 15, pp. 3308–3321, 2015.

[4] F. Sanjaya and S. Mungkasi, "A simple but accurate explicit finite difference method for the advection-diffusion equation," in *Journal of Physics: Conference Series*, vol. 909, no. 1. IOP Publishing, 2017, p. 012038.

[5] G. A. Putri, S. Hariyanto, G. A. Putri, S. Hariyanto *et al.*, "Numerical simulation of advection-diffusion on flow in waste stabilization ponds (1-dimension) with finite difference method forward time central space scheme," *Environmental Engineering Research*, vol. 23, no. 4, pp. 442–448, 2018.

[6] B. Xu, X. Zhang, and D. Ji, "A reduced high-order compact finite difference scheme based on pod technique for the two dimensional extended fisher-kolmogorov equation." *IAENG International Journal of Applied Mathematics*, vol. 50, no. 3, pp. 474–483, 2020.

[7] W. Timpitak and N. Pochai, "Numerical simulations to a one-dimensional groundwater pollution measurement model through heterogeneous soil." *IAENG International Journal of Applied Mathematics*, vol. 50, no. 3, pp. 558–565, 2020.

[8] Phongthanapanich, S. and Dechaumphai, P., "A characteristic-based finite volume element method for convection-diffusion-reaction equation," *Trans. of the CSME*, vol. 32, p. 549, 2008.

[9] Phongthanapanich, S and Dechaumphai, P, "Finite volume method for convection–diffusion–reaction equation on triangular meshes," *International Journal for Numerical Methods in Biomedical Engineering*, vol. 26, no. 6, pp. 716–727, 2010.

[10] Y. Guo, R.-x. Liu, Y.-l. Duan, and Y. Li, "A characteristic-based finite volume scheme for shallow water equations," *Journal of Hydrodynamics*, vol. 21, no. 4, pp. 531–540, 2009.

[11] F. Benkhaldoun and M. Seaïd, "A simple finite volume method for the shallow water equations," *Journal of Computational and Applied mathematics*, vol. 234, no. 1, pp. 58–72, 2010.

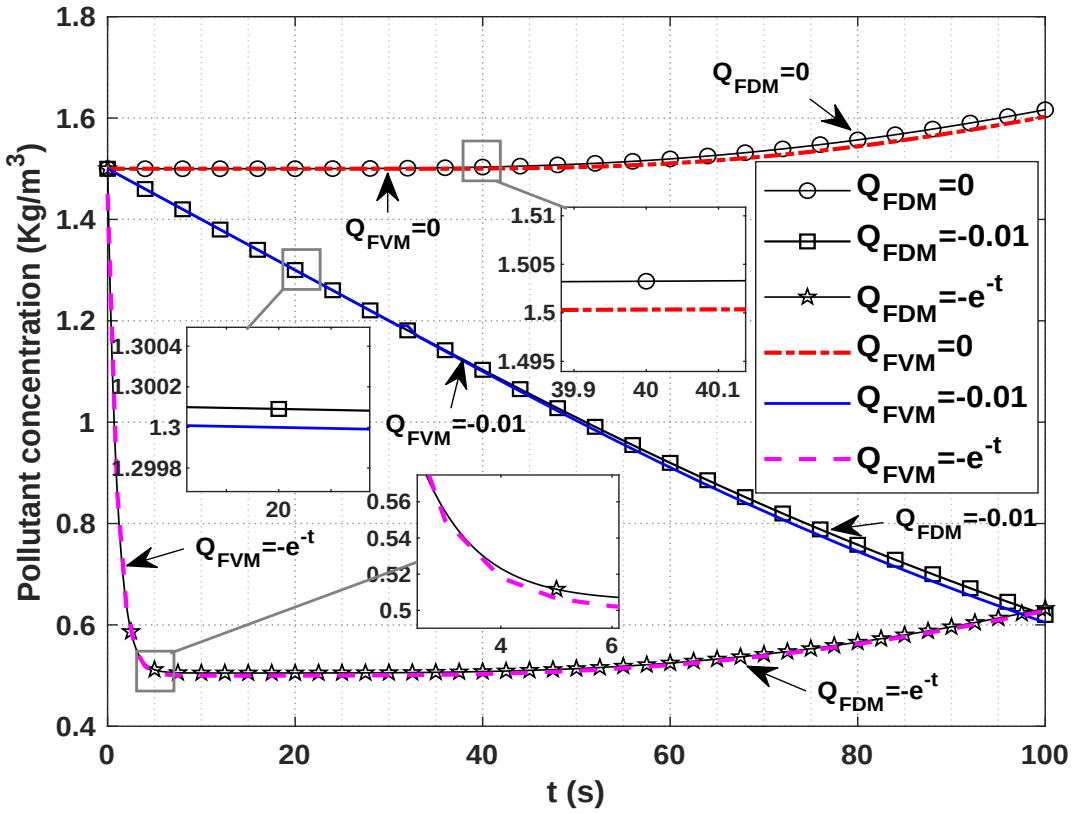

(a) midpoint of entrance gate

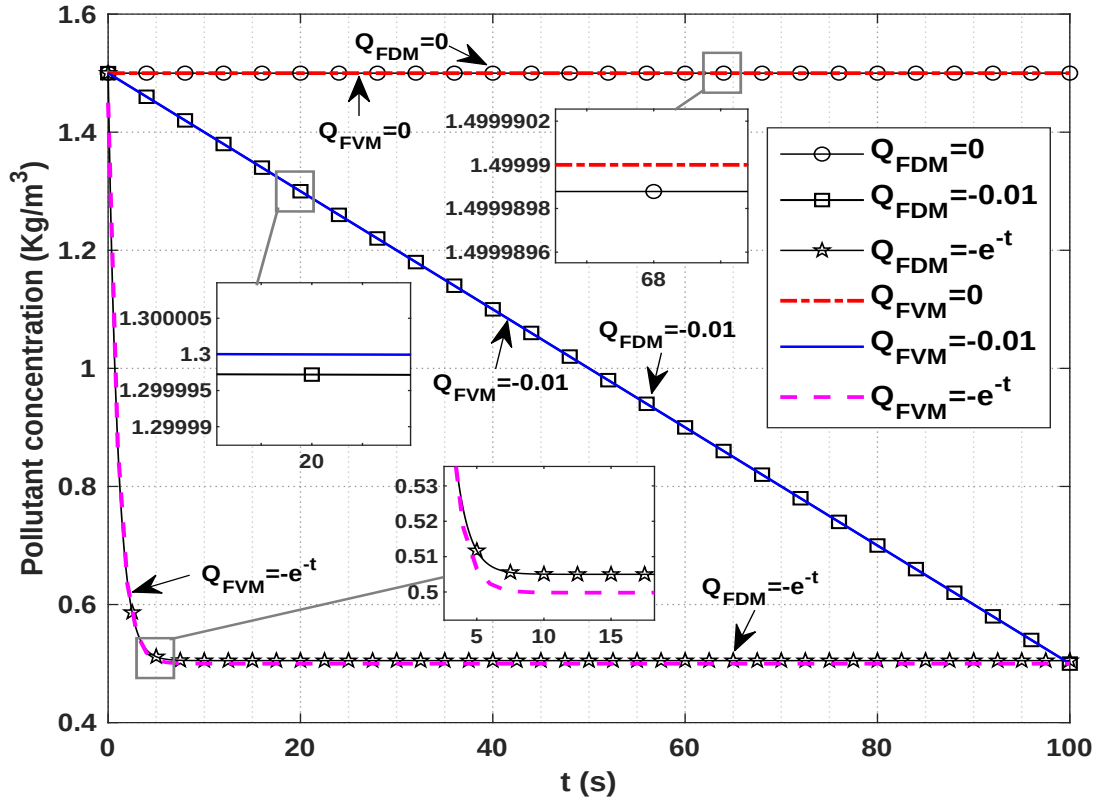

(b) midpoint between two entrance gates

Fig. 17. Comparison of the pollutant concentrations for $D_f = 50$, $x = 250$, and $y = 1000$ m with $Q = 0, Q = -0.01$ and $Q = -e^{-t}$ for (a) midpoint of entrance gate and (b) midpoint between two entrance gates.

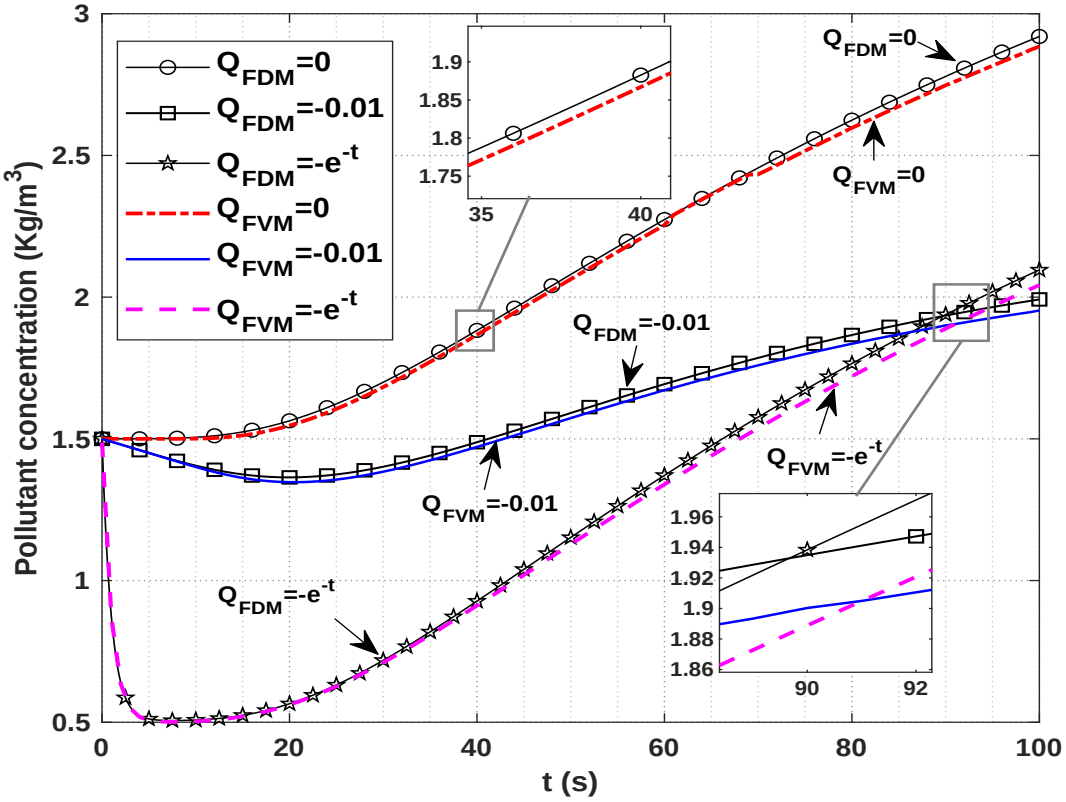

(a) midpoint of entrance gate

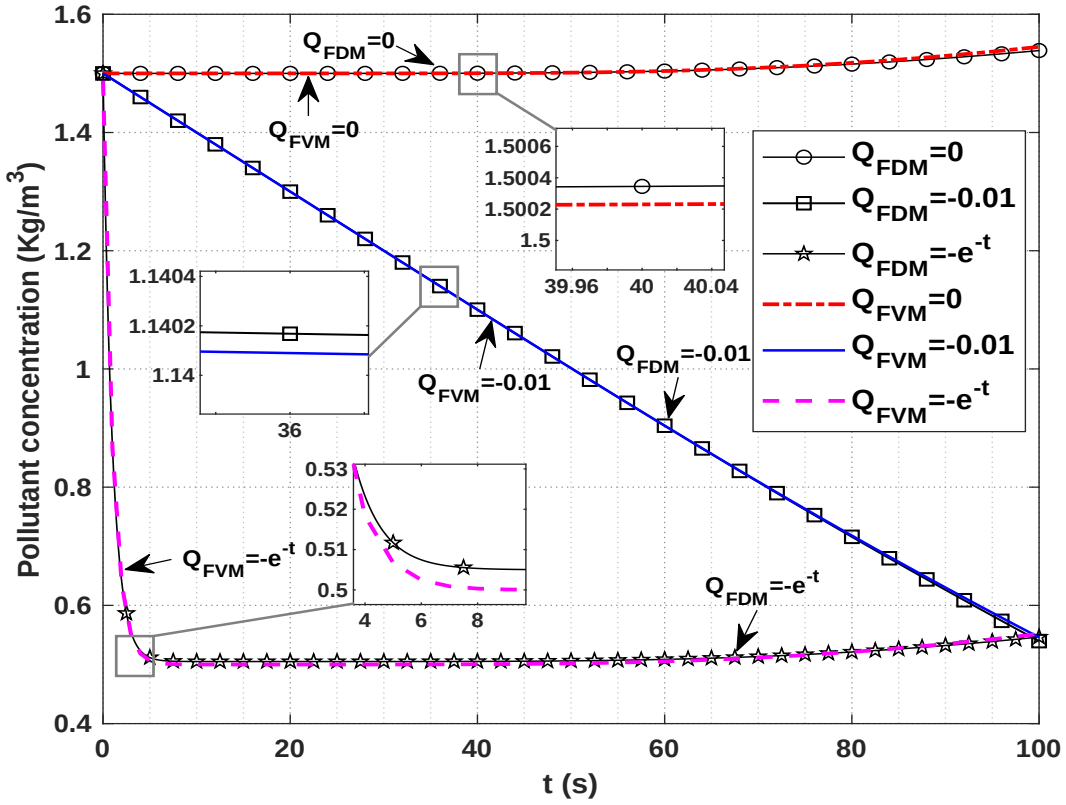

(b) midpoint between two entrance gates

Fig. 18. Comparison of the pollutant concentrations for $D_f = 200$, $x = 250$, and $y = 1000$ m with $Q = 0, Q = -0.01$ and $Q = -e^{-t}$ for (a) midpoint of entrance gate and (b) midpoint between two entrance gates.

[12] S. Phongthanapanich and P. Dechaumphai, "Explicit characteristic finite volume method for convection–diffusion equation on rectangular grids," *Journal of the Chinese Institute of Engineers*, vol. 34, no. 2, pp. 239–252, 2011.

[13] S. Phongthanapanichand P. Dechaumphai, "An explicit characteristic finite volume element method for non-divergence free convection–diffusion-reaction equation," *Int. J. Adv. Eng. Sci. Appl. Math.*, vol. 4, p. 179, 2012.

[14] T. Zhang, "Two-grid characteristic finite volume methods for nonlinear parabolic problems," *Journal of Computational Mathematics*, pp. 470–487, 2013.

[15] J. P. Arachchige and G. J. Pettet, "A finite volume method with linearisation in time for the solution of advection–reaction–diffusion systems," *Applied Mathematics and Computation*, vol. 231, pp. 445–462, 2014.

[16] W. Liu, J. Huang, and X. Long, "Coupled nonlinear advection–diffusion–reaction system for prevention of groundwater contamination by modified upwind finite volume element method," *Computers & Mathematics with Applications*, vol. 69, no. 6, pp. 477–493, 2015.

[17] C. Yang and L. M. Tine, "A hybrid finite volume method for advection equations and its applications in population dynamics," *Numerical Methods for Partial Differential Equations*, vol. 33, no. 4, pp. 1114–1142, 2017.

[18] M. Xu, "A modified finite volume method for convection-diffusion-reaction problems," *Int. J. Heat Mass Transf.*, vol. 117, p. 658, 2018.

[19] B. Lan, Z. Sheng, and G. Yuan, "A new positive finite volume scheme for two–dimensional convection-diffusion equation," *Z. Angew. Math. Mech.*, vol. 99, p. 1, 2019.

[20] T. Hafsi and F. Taallah, "Finite volume approximation of the signorini problem," *IAENG International Journal of Applied Mathematics*, vol. 49, no. 4, pp. 1–6, 2019.

[21] A. Hussain, Z. Zheng, and E. F. Anley, "Numerical analysis of convection–diffusion using a modified upwind approach in the finite volume method," *Mathematics*, vol. 8, no. 11, p. 1869, 2020.

[22] T. Goudon, F. Lagoutiere, and L. M. Tine, "Simulations of the lifshitz–slyozov equations: the role of coagulation terms in the asymptotic behavior," *Mathematical Models and Methods in Applied Sciences*, vol. 23, no. 07, pp. 1177–1215, 2013.

[23] G.-S. Jiang and C.-W. Shu, "Efficient implementation of weighted eno schemes," *Journal of computational physics*, vol. 126, no. 1, pp. 202–228, 1996.

[24] D. Anderson, J. C. Tannehill, and R. H. Pletcher, *Computational fluid mechanics and heat transfer*. CRC Press, 2016.

[25] P. Theeraek, S. Phongthanapanich, and P. Dechaumphai, "Solving convection-diffusion-reaction equation by adaptive finite volume element method," *Math. Comput. Simulat.*, vol. 82, p. 220, 2011.

[26] P. Samalerk and N. Pochai, "Numerical simulation of a one-dimensional water-quality model in a stream using a saulyev technique with quadratic interpolated initial-boundary conditions," in *Abstract and Applied Analysis*, vol. 2018. Hindawi, 2018.

[27] M. Dehghan, "Weighted finite difference techniques for the one-dimensional advection–diffusion equation," *Applied Mathematics and Computation*, vol. 147, no. 2, pp. 307–319, 2004.

[28] P. Tabuenca, J. Cardona, and A. Samartin, "Numerical model for the study of hydrodynamics on bays and estuaries," *Applied Mathematical Modelling*, vol. 16, no. 2, pp. 78–85, 1992.

[29] K. Thongtha and J. Kasemsuwan, "Numerical simulations of water quality measurement model in an opened-closed reservoir with contaminant removal mechanism," *International Journal of Differential Equations*, vol. 2018, 2018.